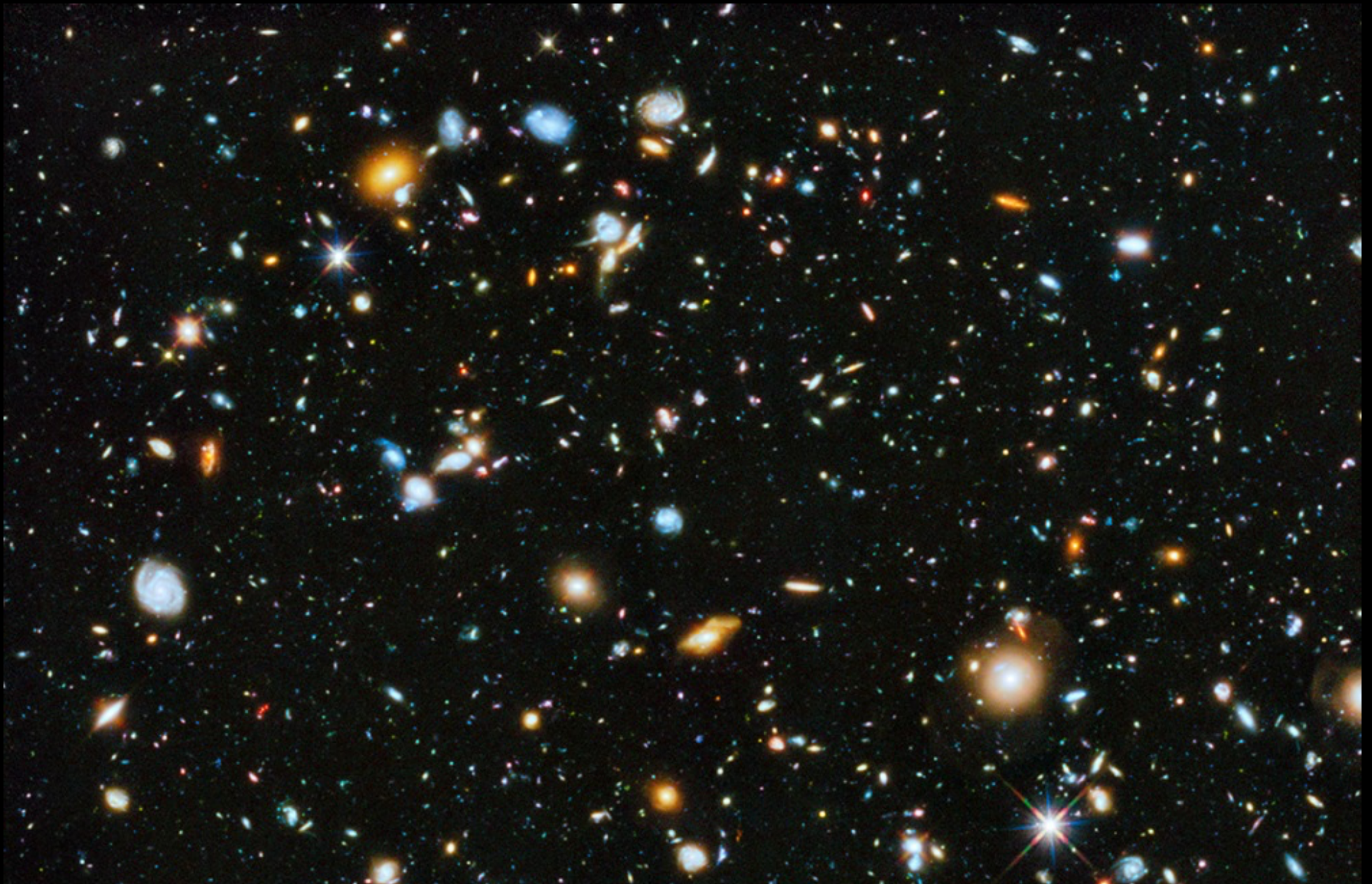


# Direct Observations of Galaxy Formation

Use observations at higher  $z$  to track  
evolution of **population**



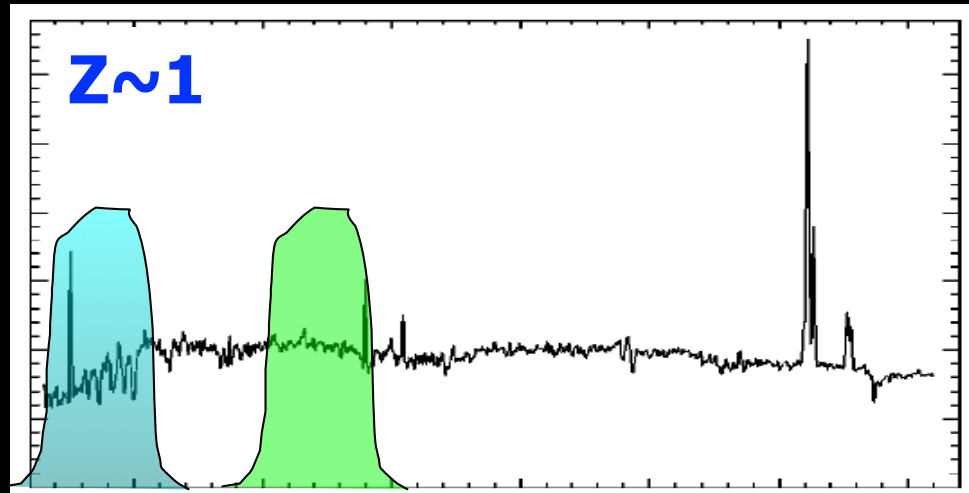
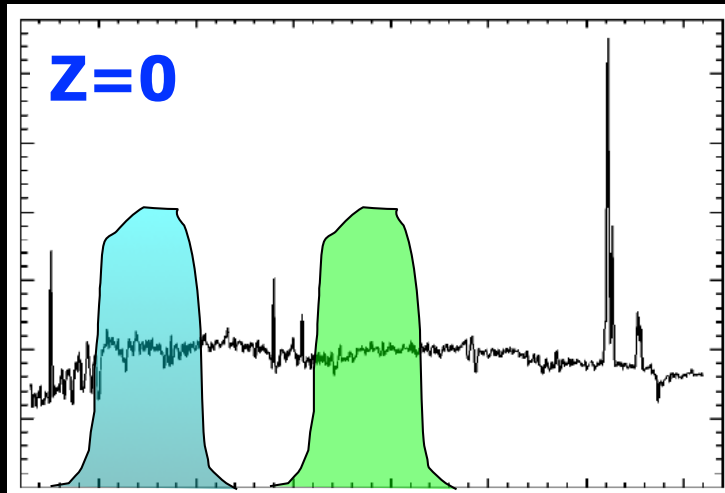
# Practicalities

- Requires significant samples with well-understood selection biases
- Can only track population — no way to know for certain what the evolutionary endpoint will be.
- Can use all the same low-z techniques to estimate physical quantities...
- BUT, be aware that local calibrations may no longer apply in very different physical conditions!

What does redshift alone do to the  
*appearance* of galaxies?

# Practicalities of dealing w/ redshift

- Observed wavelength  $\neq$  rest wavelength



$$\lambda_{\text{apparent}} \rightarrow \lambda_{\text{intrinsic}} (1+z)$$

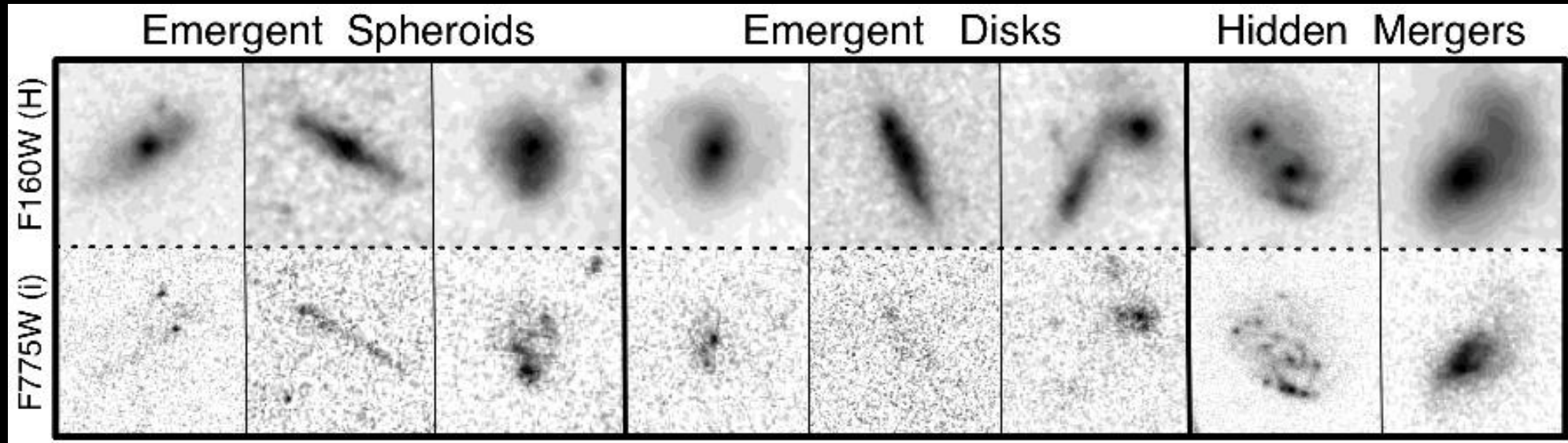
Intrinsically bluer wavelengths appear in the filter

$$\Delta\lambda_{\text{apparent}} \rightarrow \Delta\lambda_{\text{intrinsic}} (1+z)$$

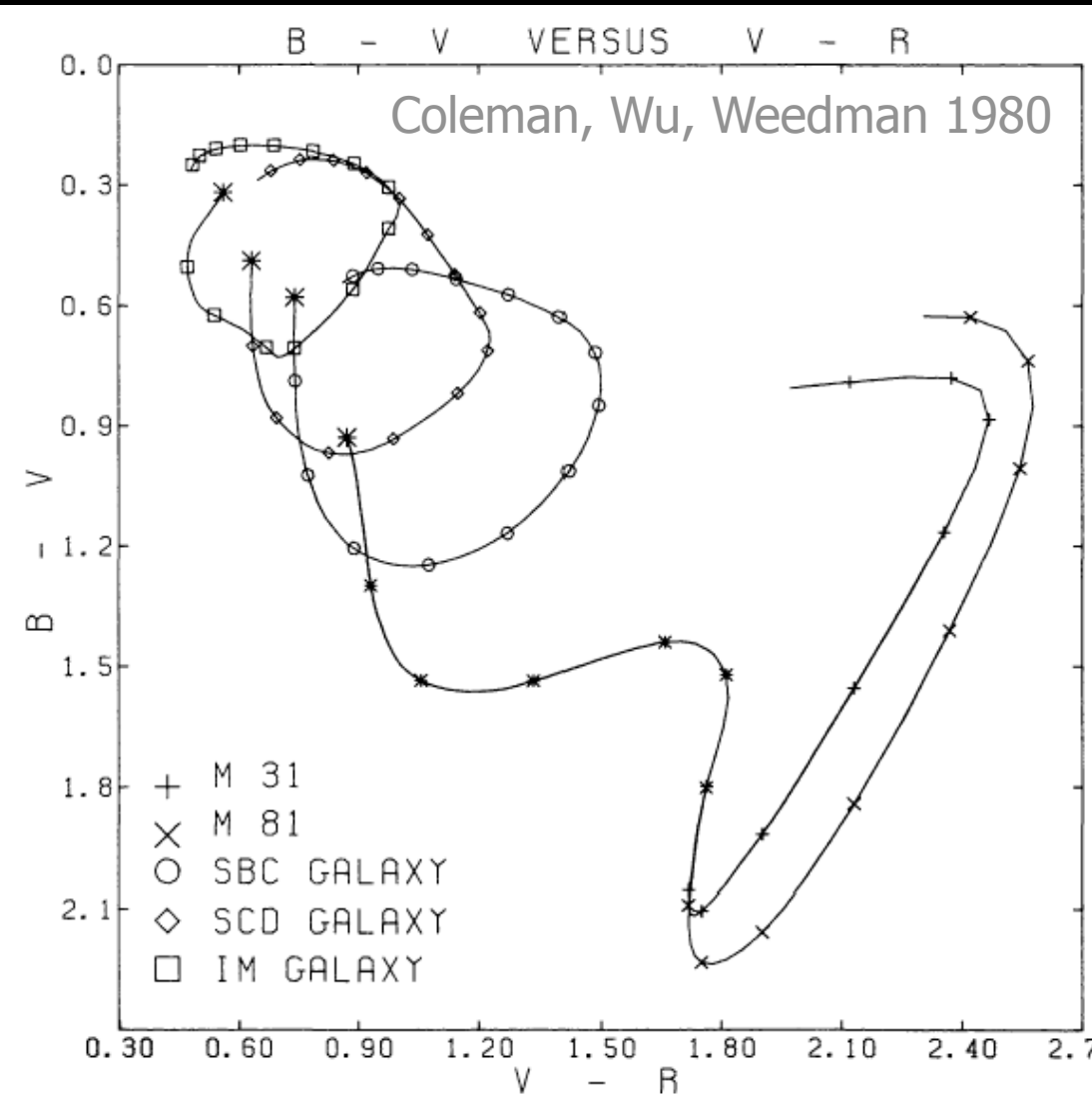
Same filter covers a smaller fraction of the spectrum

# Practicalities of dealing w/ redshift

- Galaxies are fainter:  $D_L(z)^{-2}$
- Surface brightnesses are dimmer:  $[D_A(z)/D_L(z)]^2$
- Morphology changes when looking at different rest wavelength.



# Even if spectrum is constant, apparent color+magnitude change



Different intrinsic spectra vary differently with z

FIG. 12.— $B-V$  color vs.  $V-R$  color for the five spectral energy distributions defined by Tables 2–5. Observational uncertainties are  $\pm 0.1$  to  $\pm 0.2$  mag; intrinsic differences among galaxies of the same type can be greater (see Figs. 14–20). Symbols occur at intervals of 0.1 in redshift.

# Strategies for constructing redshift-independent magnitudes:

- Adjust choice of filters to compare same rest-frame wavelengths (u at  $z=0$ , r at  $z=1$ )
- Estimate underlying SED, and “k-correct” magnitude to consistent rest-frame wavelength

# Definition of the “k-correction”

Consider a source observed to have apparent magnitude  $m_R$  when observed through photometric bandpass  $R$ , for which one wishes to know its absolute magnitude  $M_Q$  in emitted-frame bandpass  $Q$ . The  $K$  correction  $K_{QR}$  for this source is *defined* by

$$m_R = M_Q + DM + K_{QR} , \quad (2)$$

where  $DM$  is the distance modulus, defined by

$$DM = 5 \log_{10} \left[ \frac{D_L}{10 \text{ pc}} \right] , \quad (3)$$

where  $D_L$  is the luminosity distance (e.g., Hogg 1999) and  $1 \text{ pc} = 3.086 \times 10^{16} \text{ m}$ .

Hogg et al 2002; astro-ph/0210394

Note: There are other definitions floating around. A common one has a factor of  $(1+z)$  taken out, to account for the bandpass stretching, which is independent of the shape of the underlying spectrum

$$k_B(z) = B(z) - B(z=0) - 2.5 \log(1+z).$$

Frei & Gunn 1994

# Different underlying spectra will have different k-corrections, in different filters, at different redshifts

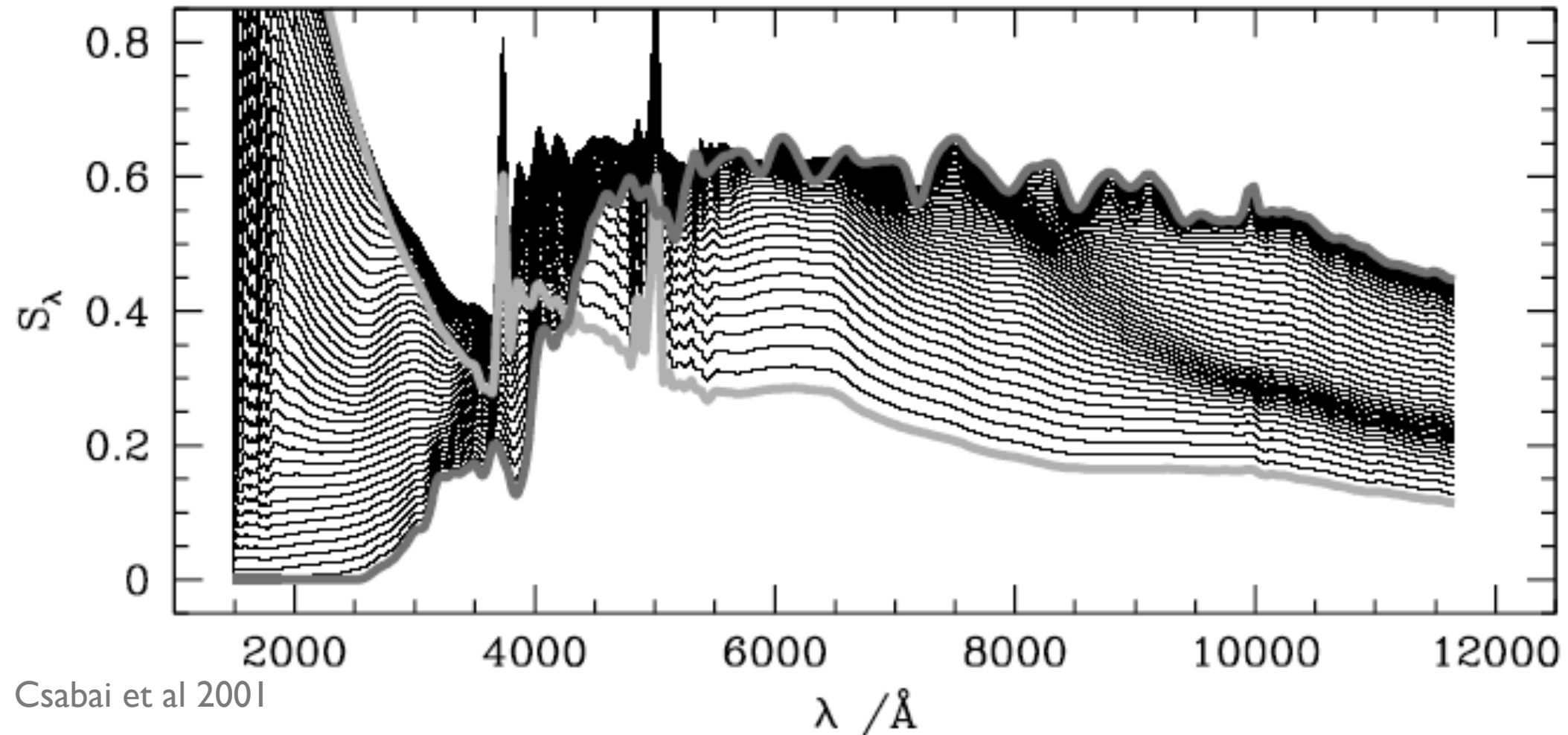


Fig. 12.— Illustration of the 1D type manifold. A few SEDs are plotted here for a equally spaced type parameter values. The reddest and bluest SEDs are shown with the thick dark and light grey curves, respectively.

# k-corrections

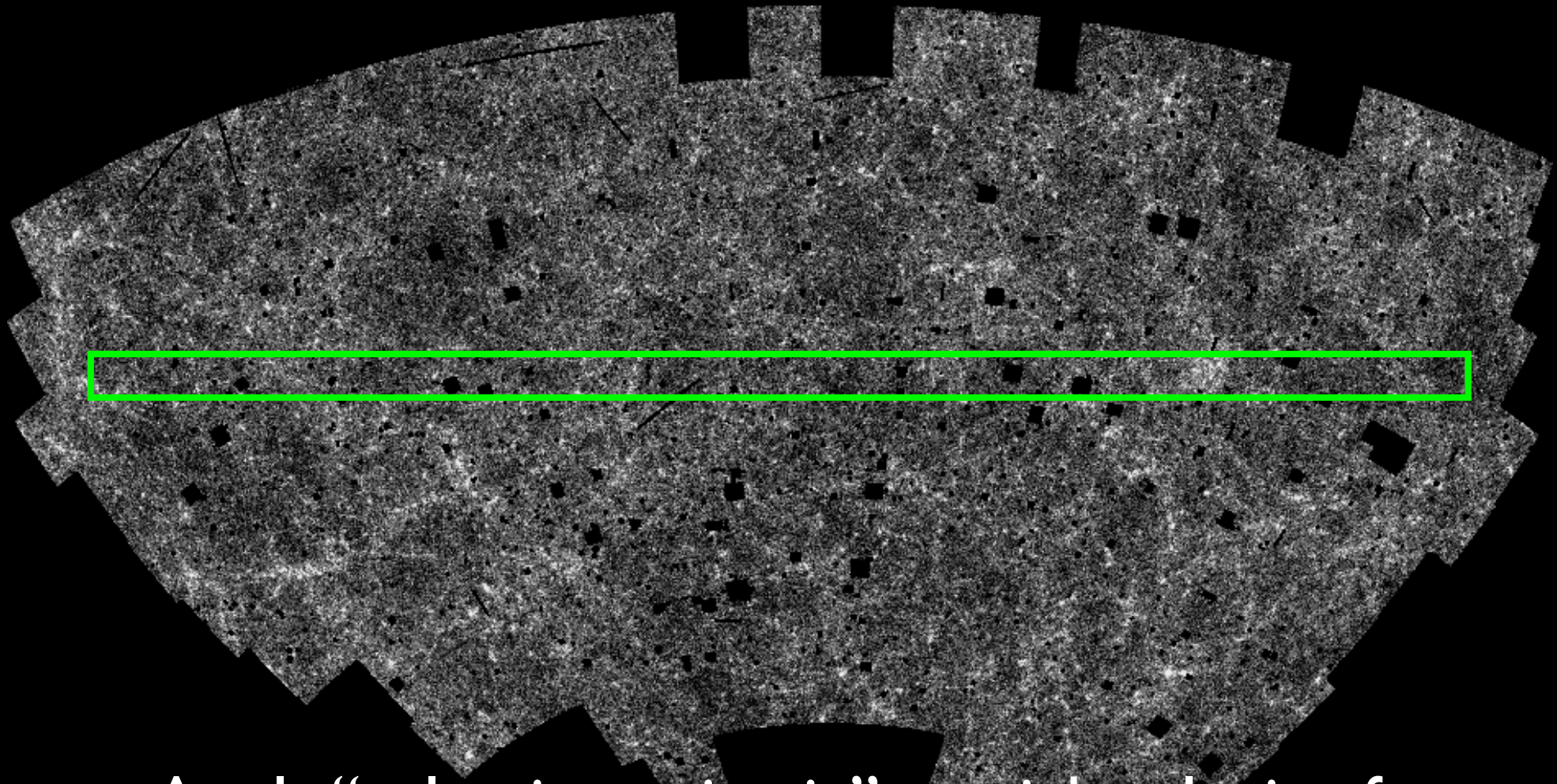
- Usually make galaxies fainter than expected
  - Most spectra fall towards UV, so looking at dimmer part of spectra
- Corrections smaller and less variable in NIR
  - Power-law side of stellar black bodies
- Depends on dust
  - Anything that affects the spectrum changes the k-correction
- Can be negative in the submillimeter
  - Peak of cool dust black-body moves into band-pass.

How do we find galaxies at different redshifts?

# Finding Redshifted Galaxies

- Brute force — measure lots of redshifts
- Photometric redshifts
  - galaxies
  - QSO's
  - including dust+IGM absorption
- Selecting high-z galaxies
  - Dropout techniques (“Lyman Break Galaxies”=LBG)
  - Selecting non-SF galaxies (NIR, BzK)
  - Lyman-alpha emitters
  - Sub-mm galaxies

# I. Brute force spectroscopy: “redshift surveys”



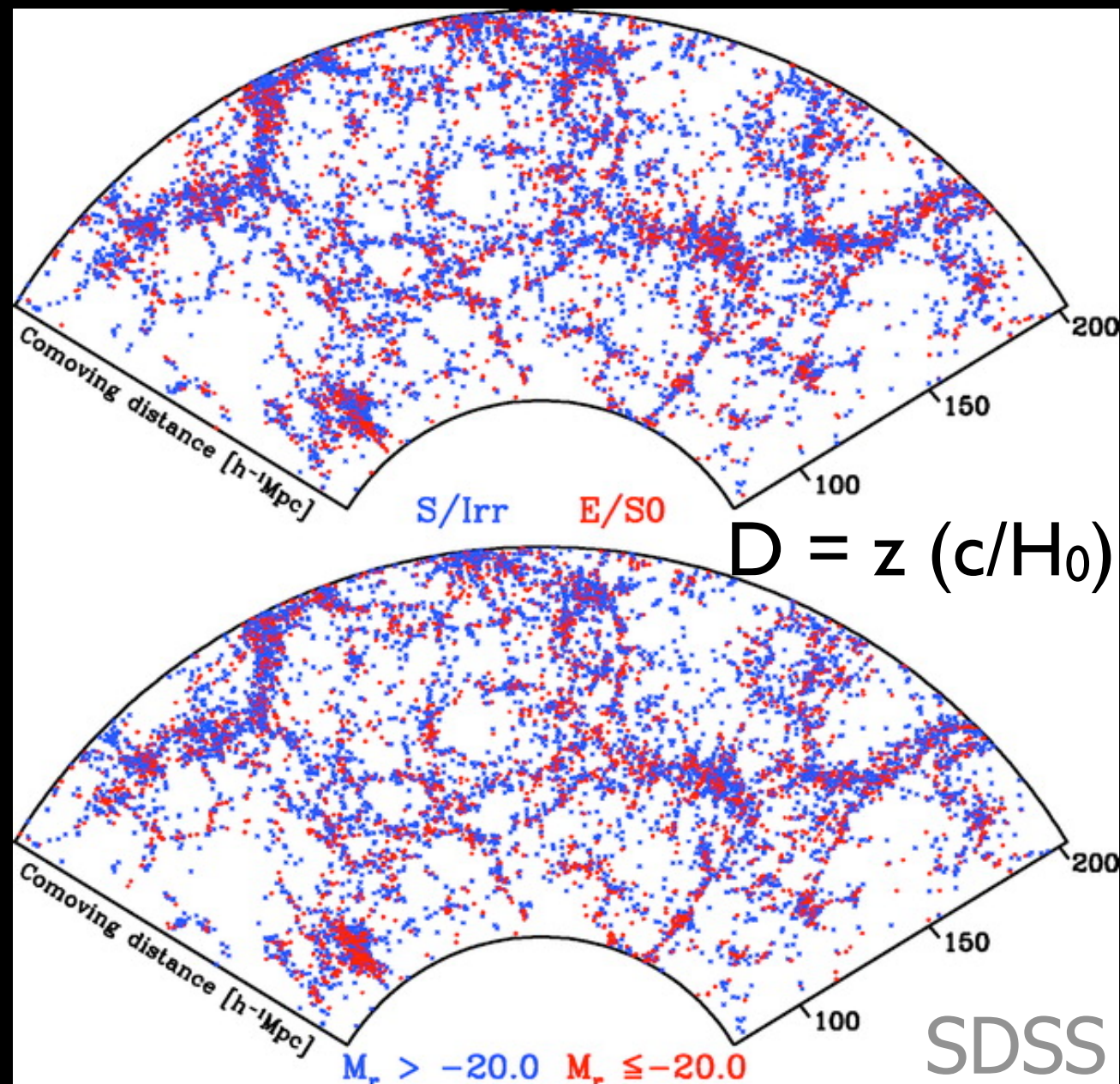
Apply “selection criteria” to pick galaxies for spectroscopy (i.e. all galaxies above a fixed magnitude in some filter, in some area of the sky)

# Redshift surveys: Probe galaxy population and clustering simultaneously

*Morphology:*  
Ellipticals more clustered

*Luminosity:*  
Fainter galaxies less clustered

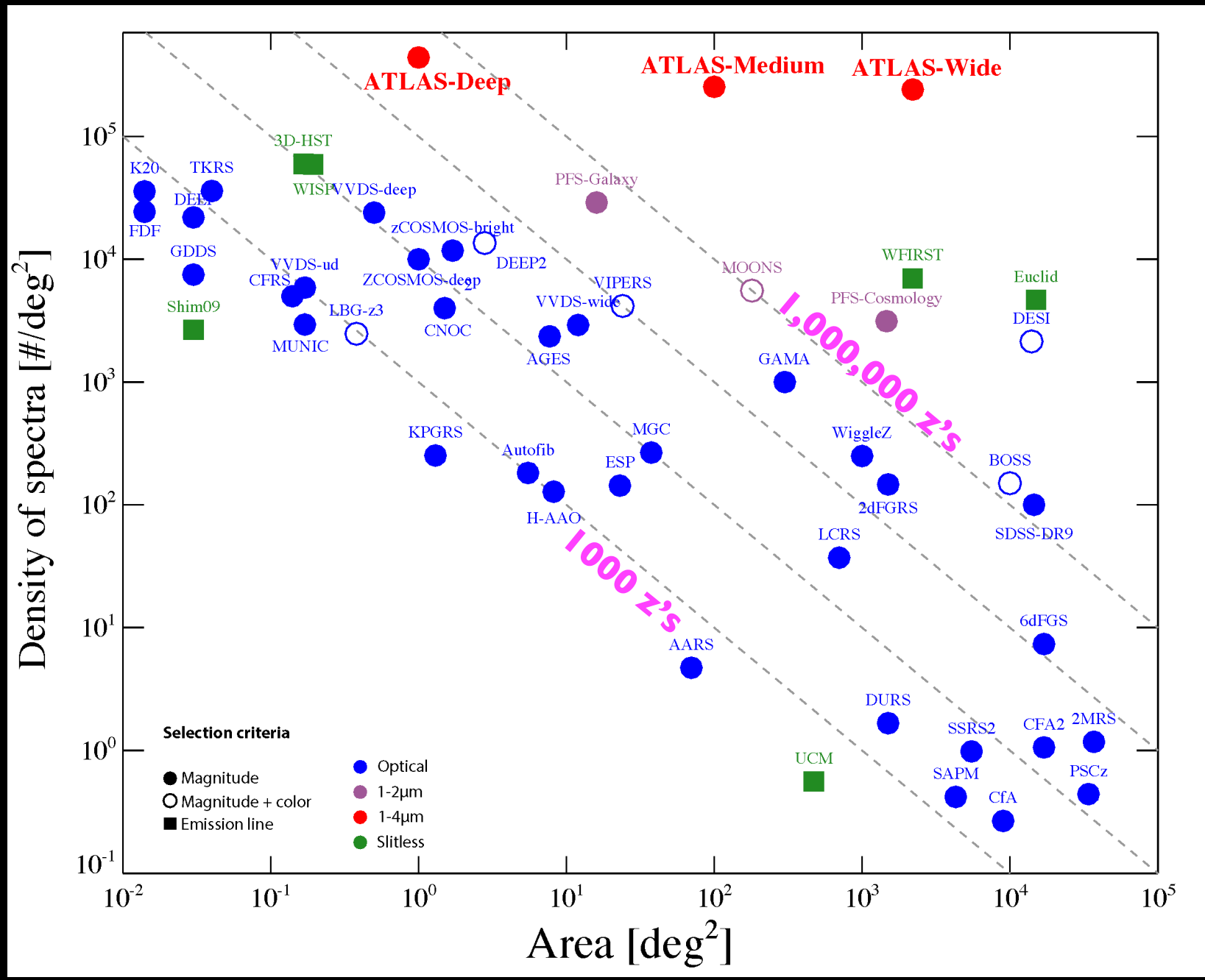
Stretching along line of sight is due to high doppler velocities in galaxy clusters  
(i.e.,  $z = z(\text{Hubble}) + z(\text{doppler})$ )



SDSS

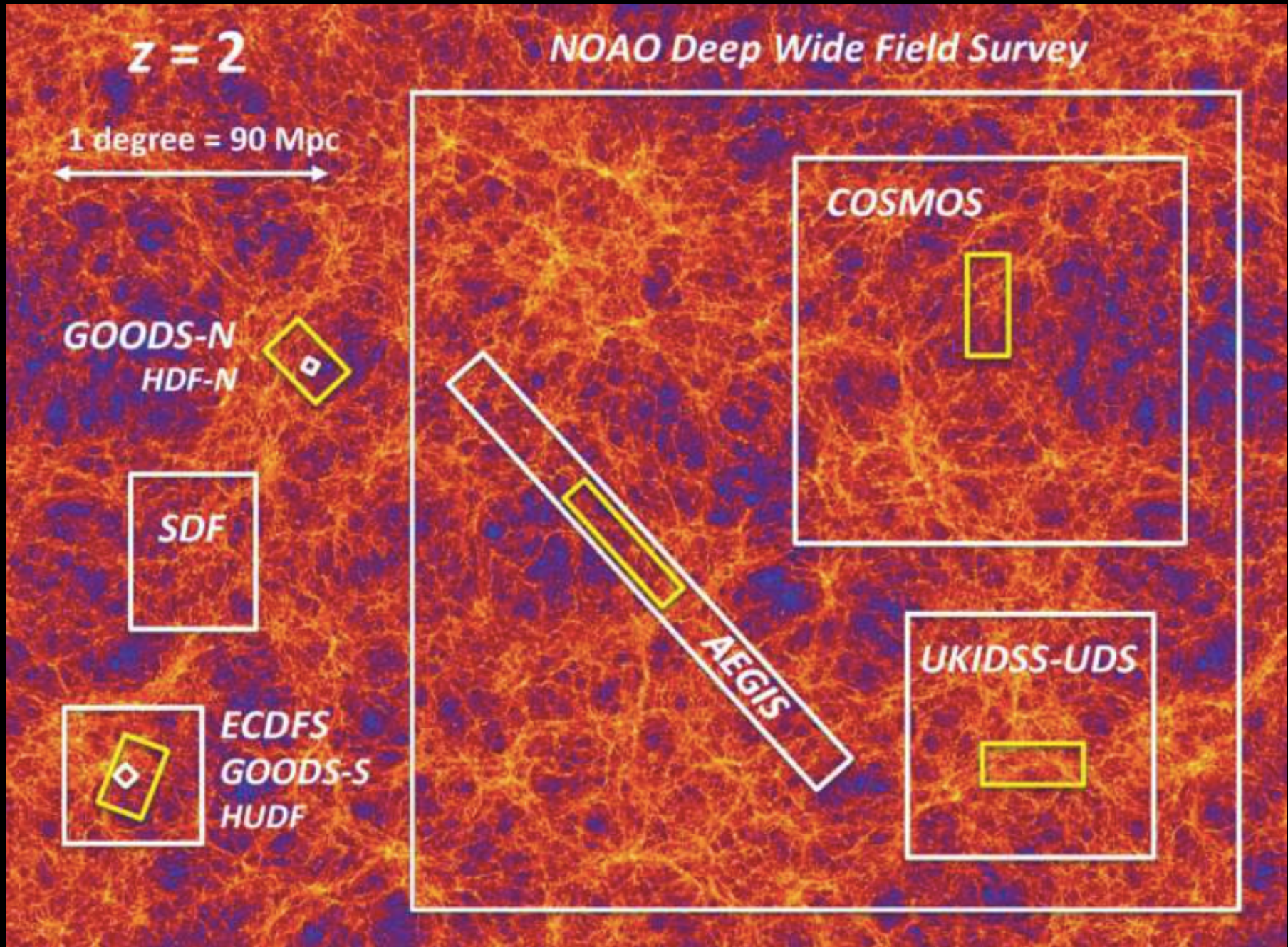
# Redshift surveys: always after more!

Higher density of spectra usually means fainter magnitude  
limit and thus more distant galaxies



Wang et al 2018; Diagonal lines are constant numbers of spectra

# Deep redshift surveys often target where there is deep, high-quality imaging data



## 2.“Photometric Redshifts” (or “photo-z’s”): Fit measured magnitudes with redshifted SED

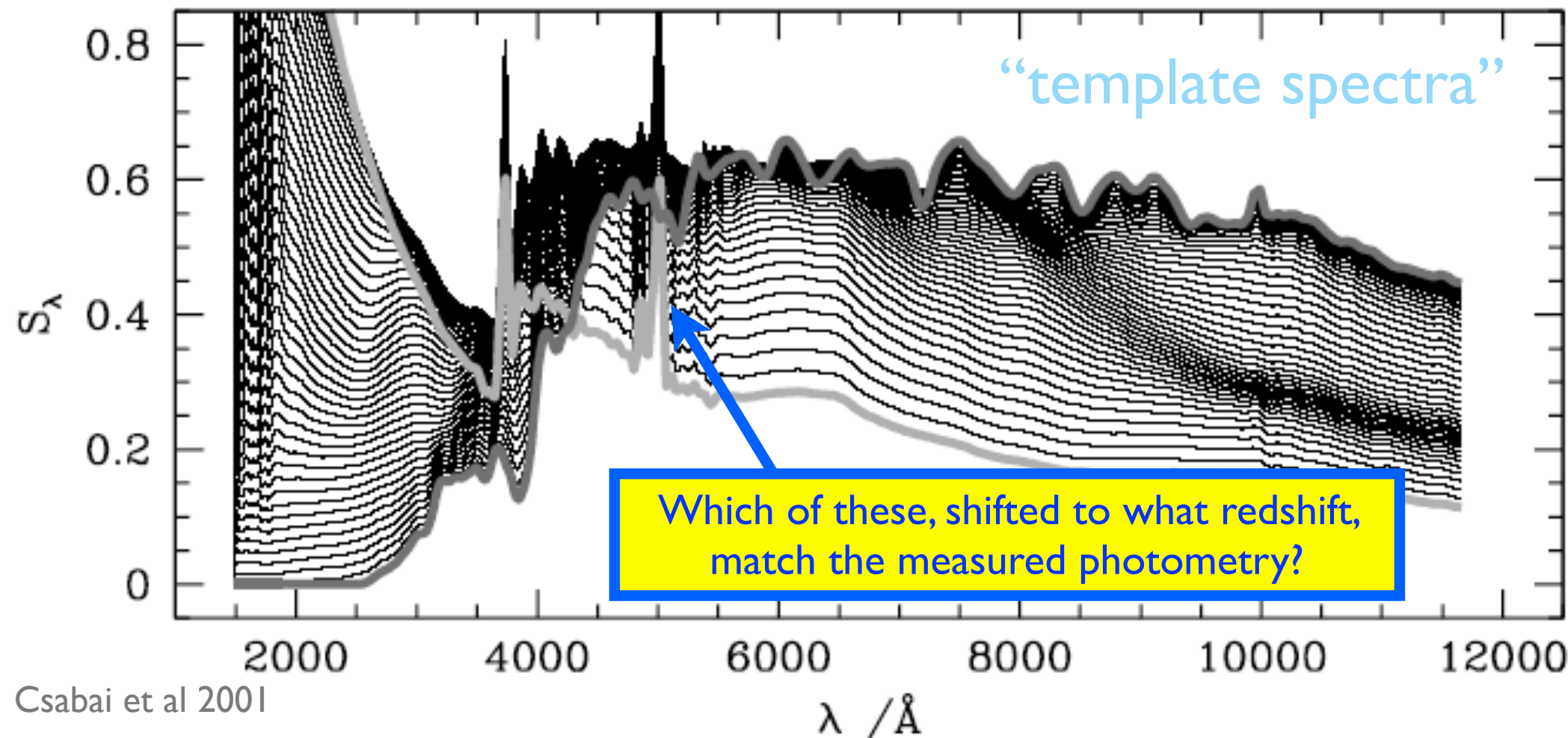
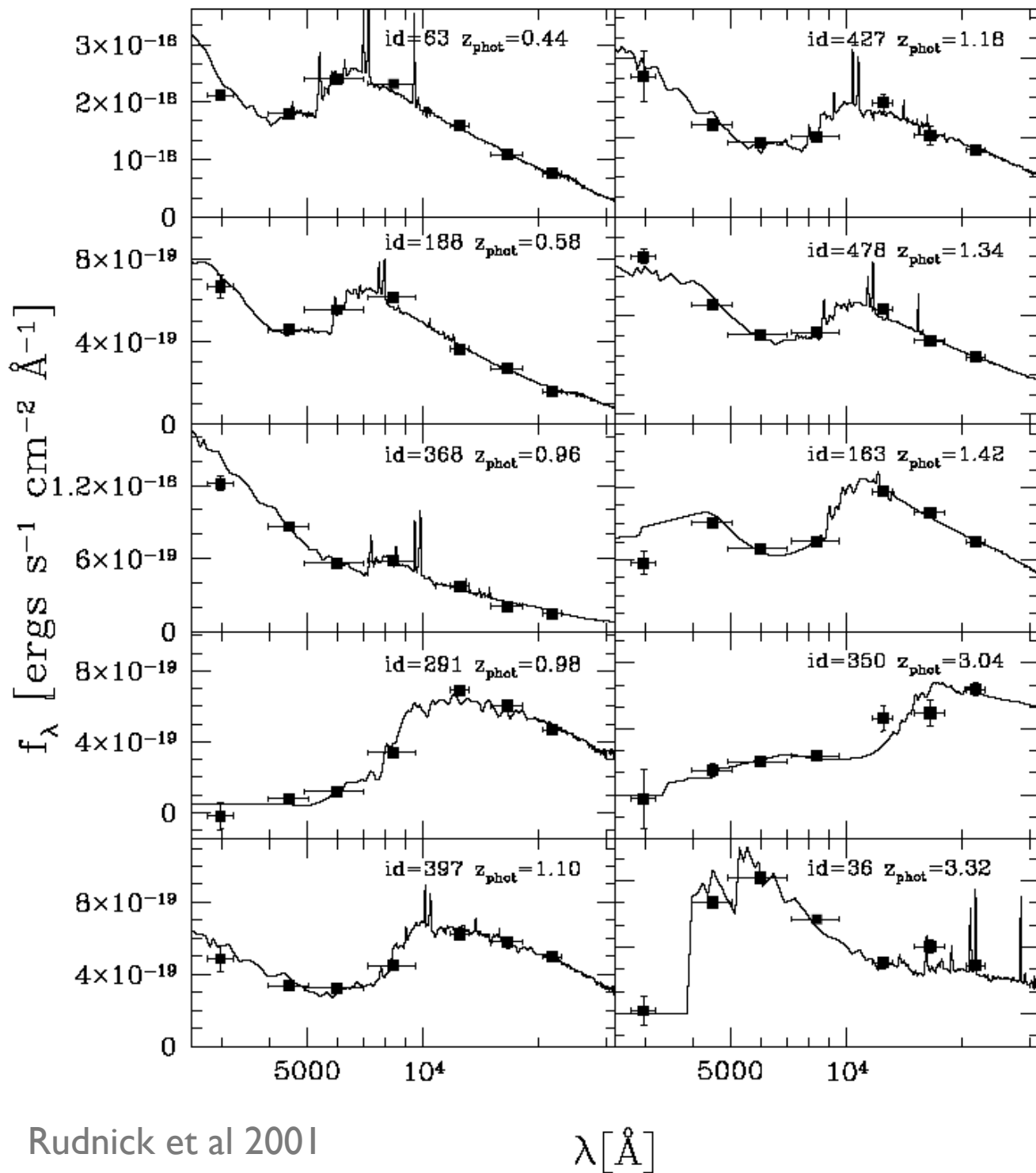


Fig. 12.— Illustration of the 1D type manifold. A few SEDs are plotted here for a equally spaced type parameter values. The reddest and bluest SEDs are shown with the thick dark and light grey curves, respectively.

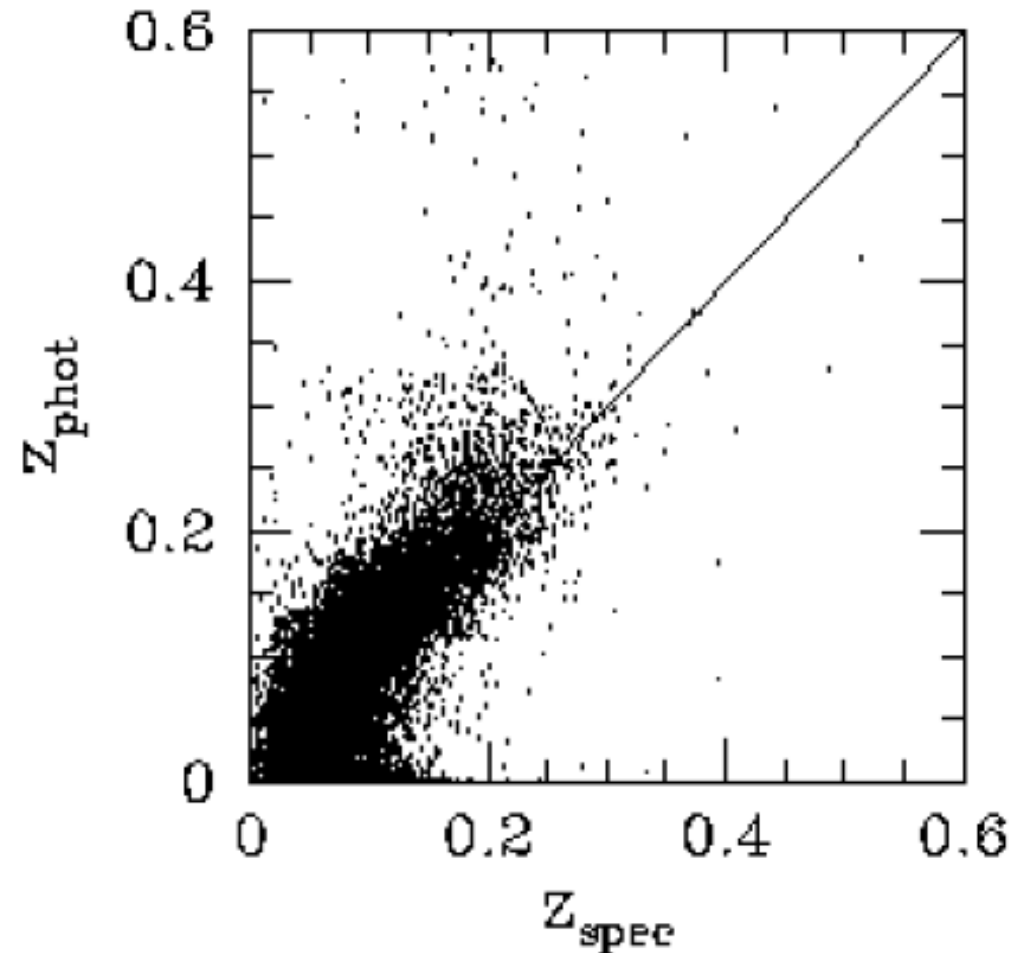
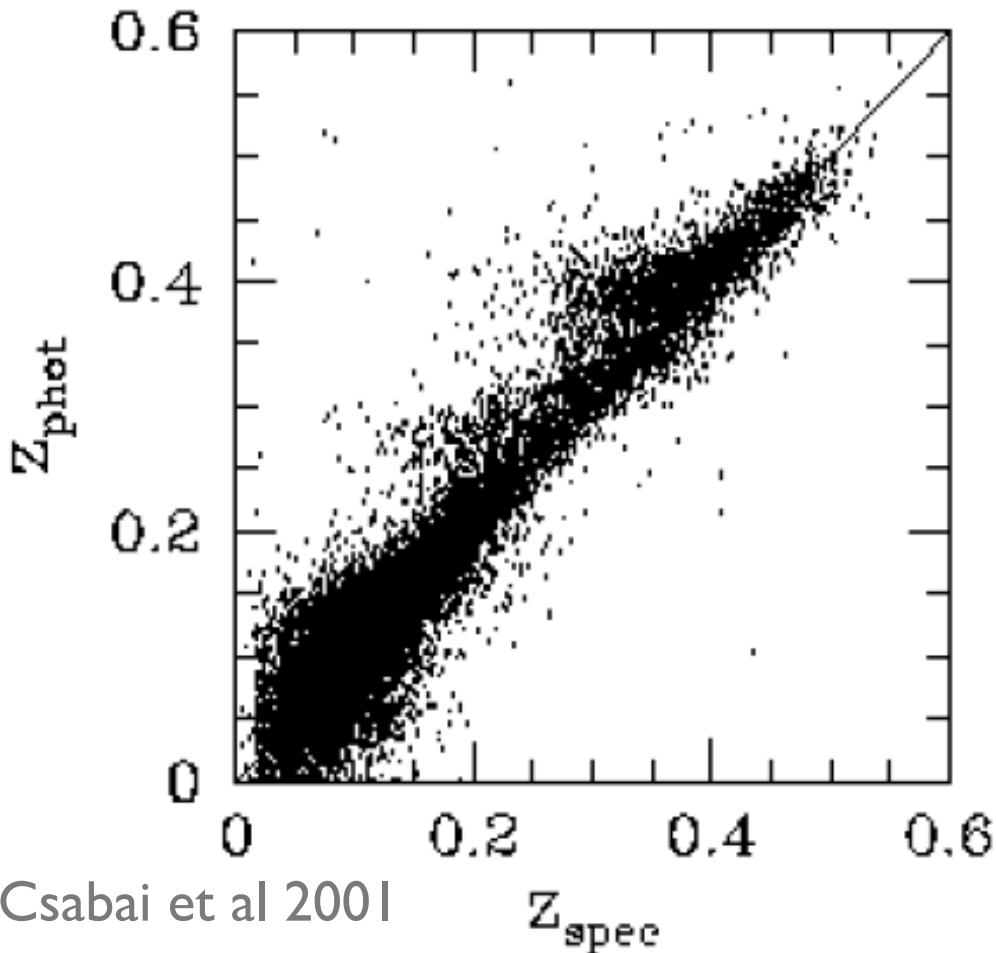


Take a wide range  
of filters (UV-NIR  
best) and fit the  
observed SED  
with redshifted  
template spectra

Template also  
constraints:  
SFR  
Stellar Mass  
Extinction

FIG. 5.—Sample of template fits to photometric data for 10 objects in the HDF-S. The measured  $z_{\text{phot}}$  increases down and to the right. In addition to blue, star-forming galaxies, there are many galaxies at  $z > 1$  with strong Balmer or 4000 Å breaks.

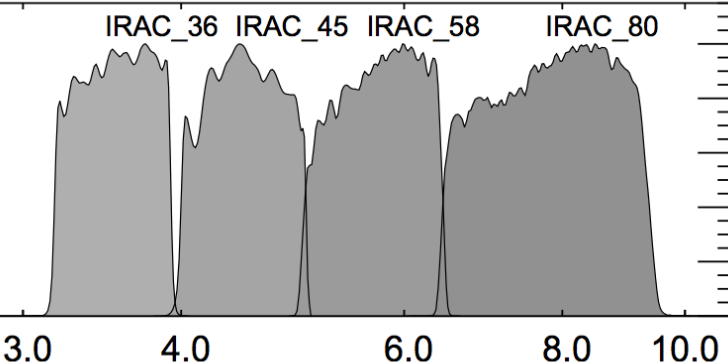
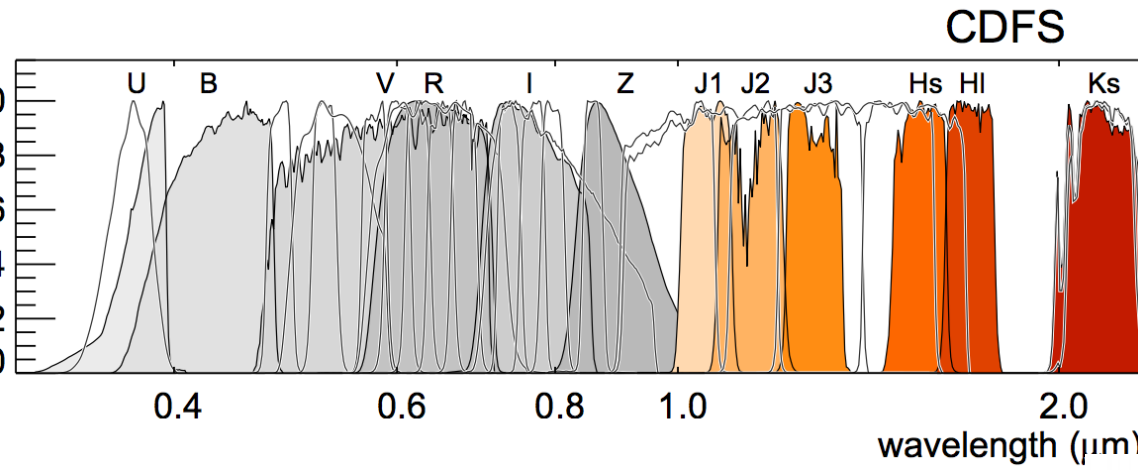
Photo-z's are good to 0.01-0.1, with some catastrophic failures.



SDSS optical photo-z's (left: **red galaxies**; right: **blue galaxies**)

(Failures can be catastrophic though -- errors are non-Gaussian.  
For wider ranges in  $z$ , NIR usually required for accuracy)

Normalized transmission



More, narrower filters can significantly improve accuracies.

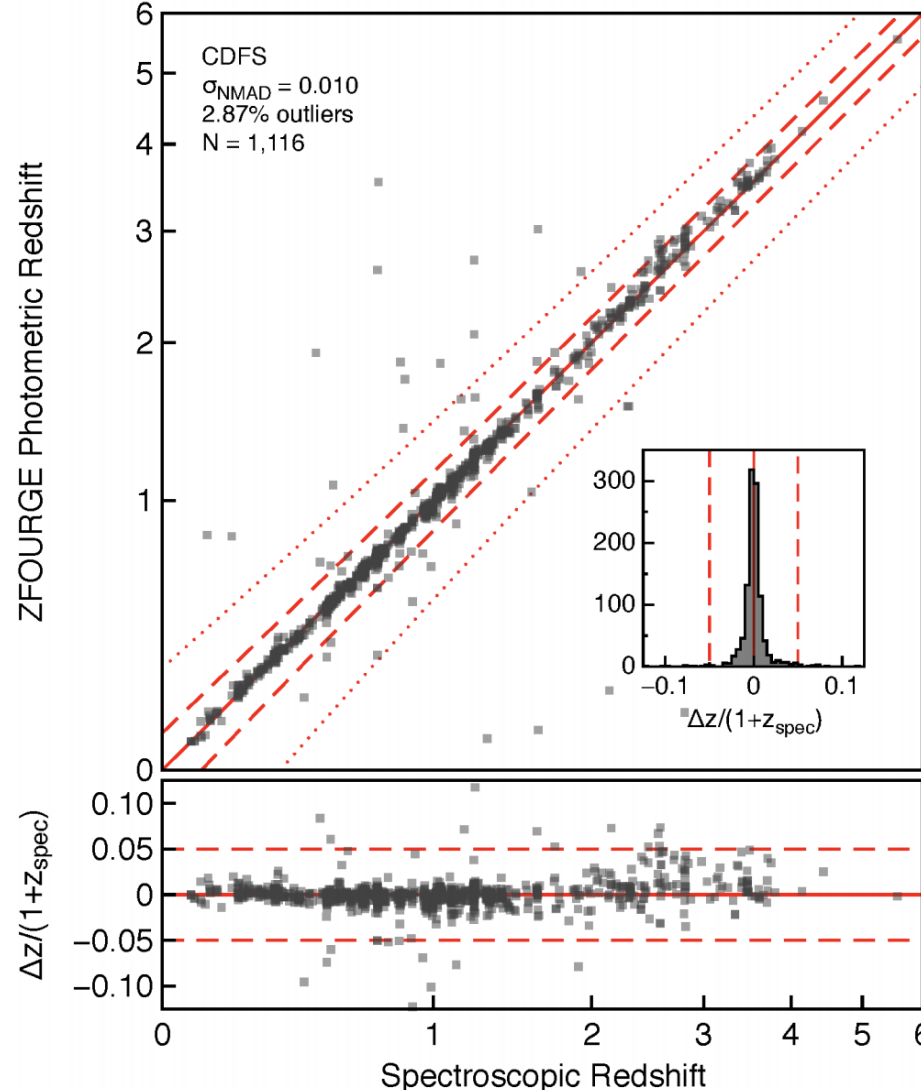


# Photo-z's for QSOs: Get z and classification

← Increasing Redshift

$\text{Ly}\alpha$  is strongest line  
and moves into the  
optical at  $z \sim 2.5$

Broader, different lines,  
different continuum shape  
than galaxies

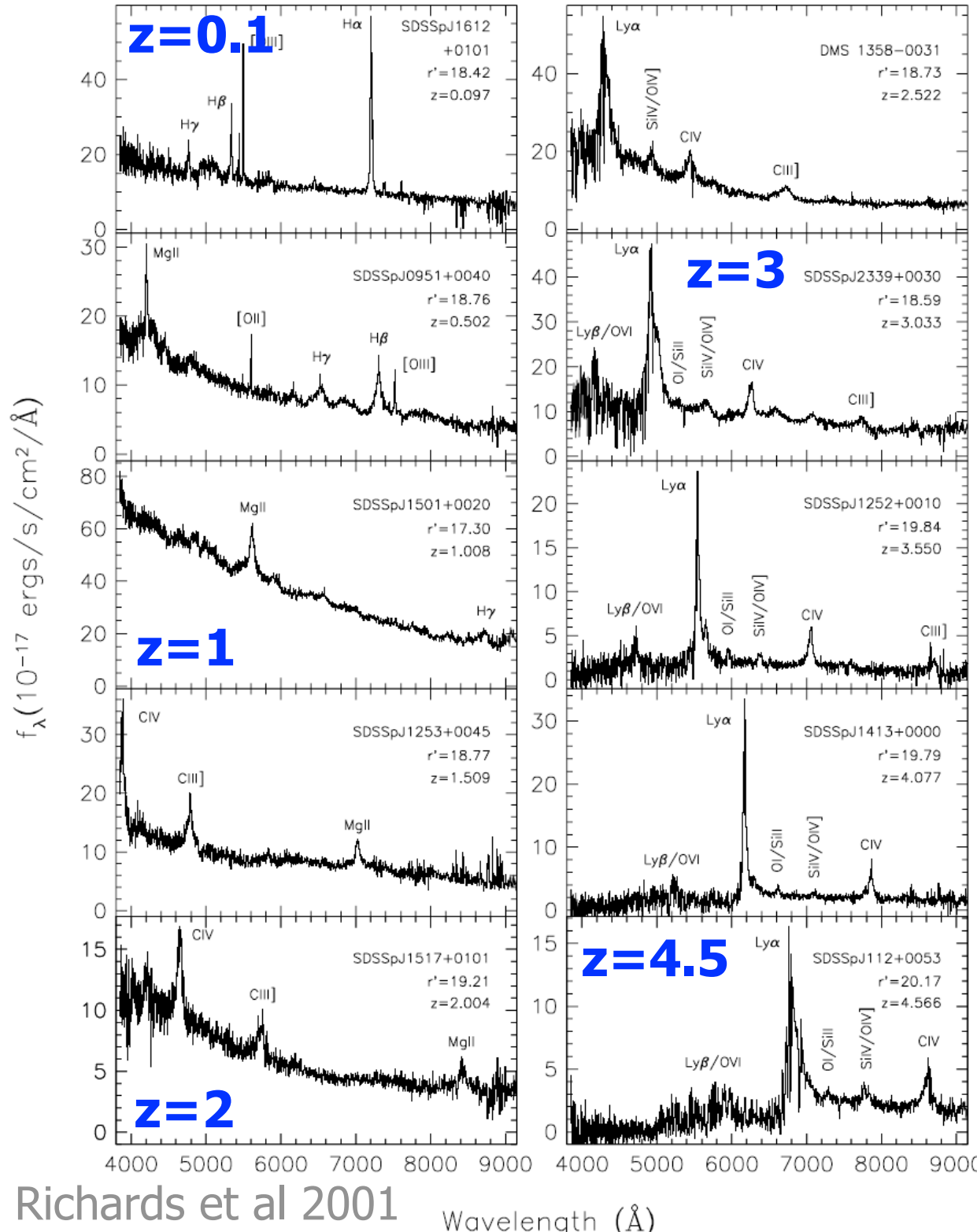
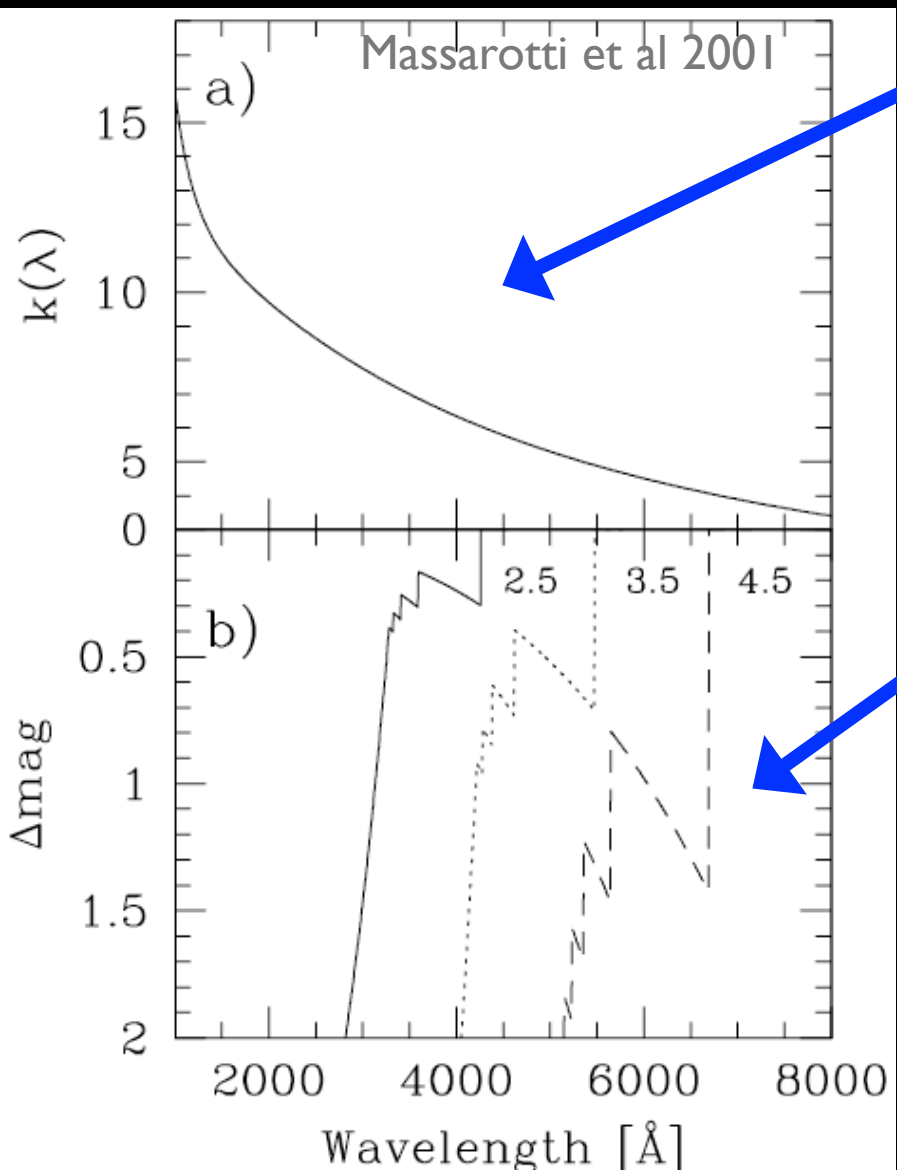


# Photo-z's: Need to include dust + IGM



**Dust:** probably increasingly important at higher  $z$ , where a larger fraction of galaxies seem to be in the “starburst” (i.e. ULIRG) mode, Metallicity lower, though.

**IGM:** Ly- $\alpha$  absorption from hydrogen along the line of sight to the distant galaxy produces sharp “breaks” in the spectra, and absorbs all photons bluer than a certain wavelength

**Fig. 2.** Panel a) the adopted dust attenuation law after Calzetti (1999). Panel b) the IGM attenuation in a magnitude scale at redshift 2.5, 3.5 and 4.5, as labelled, according to Madau (1995)

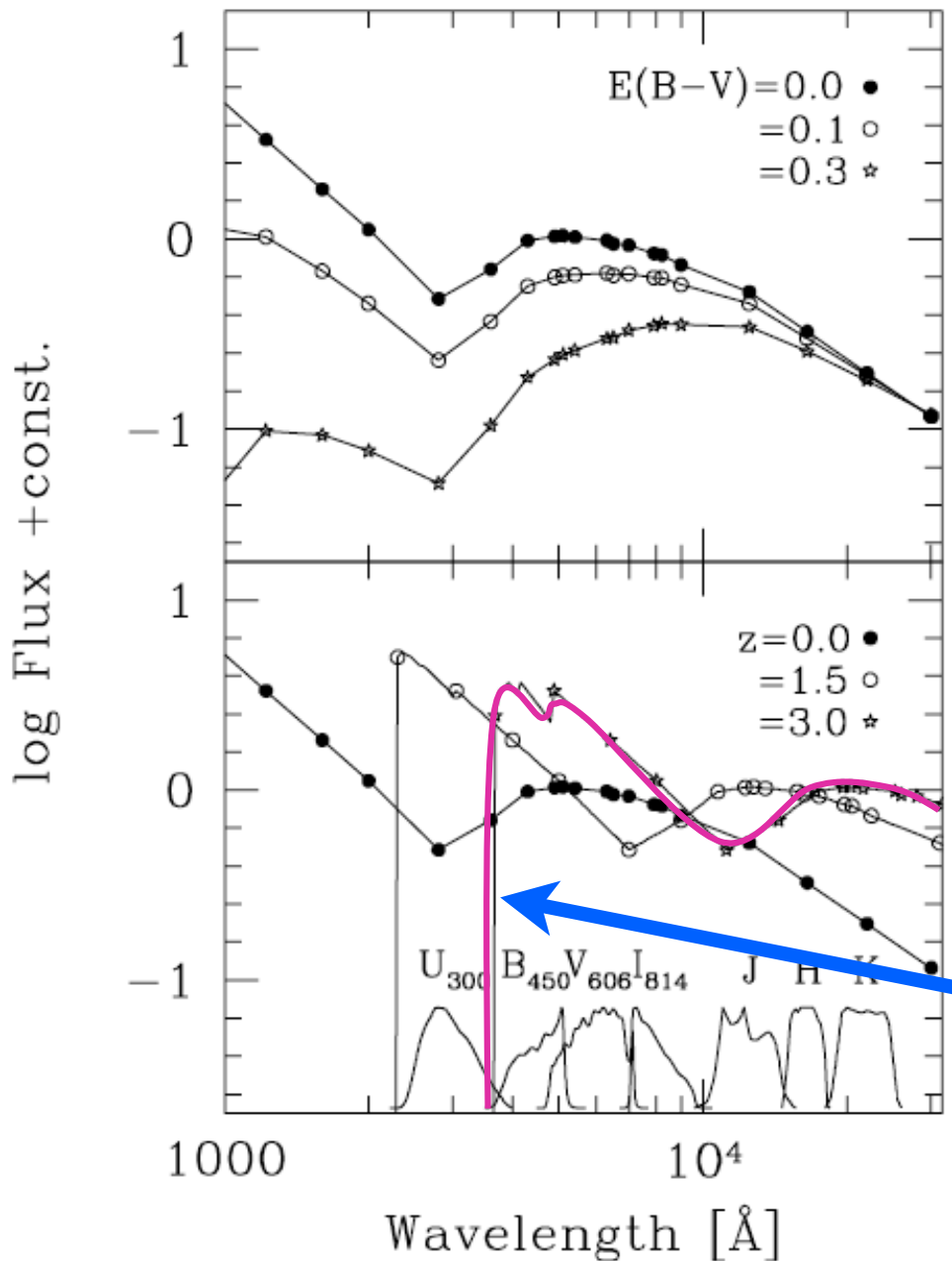
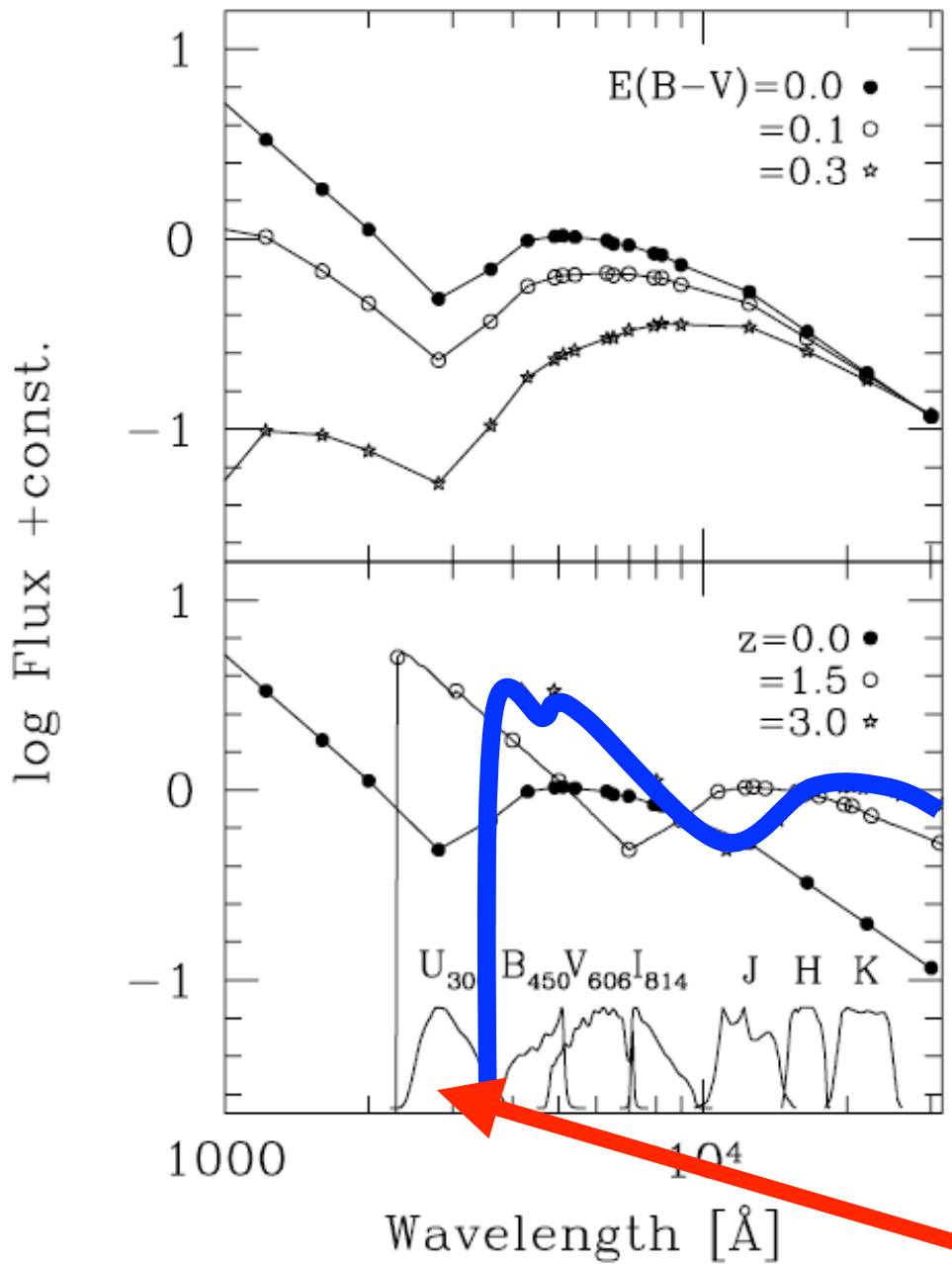


**Fig. 3.** The effect of internal reddening and IGM on the Sb reference template from Buzzoni (2000). Dust attenuation for  $E(B - V)$  up to 0.3 mag, as labelled, is shown in the upper panel, while the expected break induced by the Ly- $\alpha$  forest at  $z = 1.5$  and  $z = 3$  is shown in the lower panel. For reference, the HST photometric system and the Johnson *JHK* bands are displayed at the bottom

# Examples of the effects of dust (top) and IGM absorption (bottom) on a typical starburst spectrum

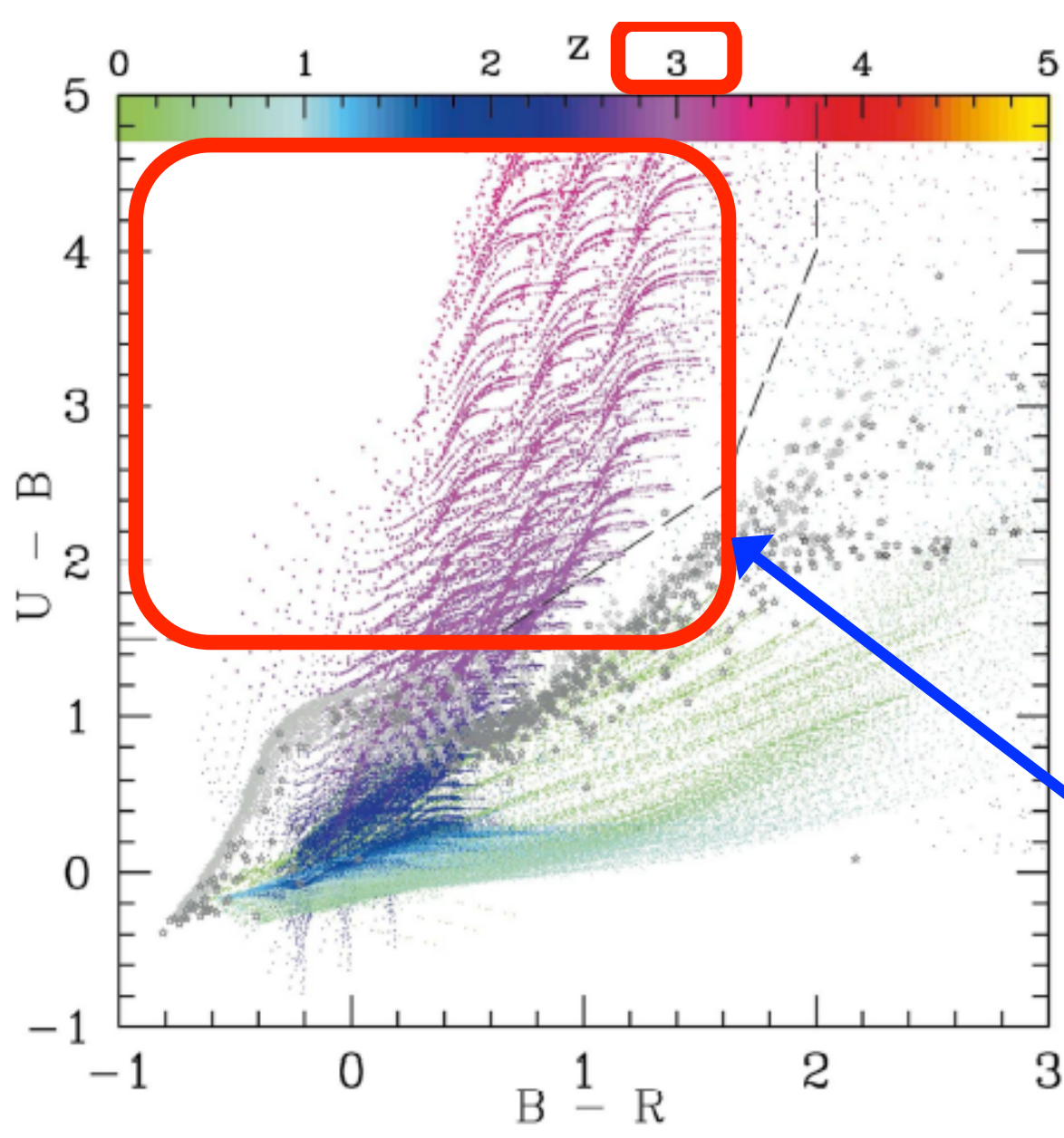
IGM absorption at Lyman edge puts a very sharp feature in the overall SED



### 3. “Lyman Break Technique”:

Use feature produced by IGM Ly $\alpha$  absorption to identify high-z galaxies

No flux in U-band: “U band drop out”



$z \sim 3$  galaxies are extremely red in  $U - B$ , solely due to IGM

Few galactic stars or other galaxies fall in this color region.

**Figure 5.** Variation of  $U - B$  and  $B - R$  colours with redshift  $z$ . Galaxies are indicated by small dots coloured by redshift; young (age  $< 100$  Myr) galaxies in the redshift range  $2.75 < z < 3.5$  have been emphasized. The colours of galactic stars have been superimposed: light grey stars are those from the model data of Bessell, Castelli & Plez (1998), while the darker grey stars are from the photometric standards of Landolt (1992). Black stars represent M dwarfs and use data obtained from Bessell (1991) and Leggett (1992). Our selection criteria are indicated by the dashed lines. A broad area of colour–colour space is enclosed, allowing for efficient selection of candidate high-redshift galaxies in spite of photometric errors, as long as a sufficiently large break in  $U - B$  can be observed. In practice this is the limiting factor, owing to the relatively poor quantum efficiency  $U$  of the TEK CCDs used compared with that of more modern detectors. Galaxies at redshifts above  $z \approx 3.5$  will have almost complete absorption in  $U$  and thus extreme  $U - B$  colours off the top of this plot, but in practice we will only measure lower limits to this colour. As redshift increases, increasing absorption in  $B$  will push  $B - R$  further towards the red. Making the upper bound to the cut in  $B - R$  (or more generally for the two longer wavelength bandpasses) further to the red allows for selection of objects at higher redshifts than are shown on this plot, however this must not be pushed so far as to reach the stellar locus.

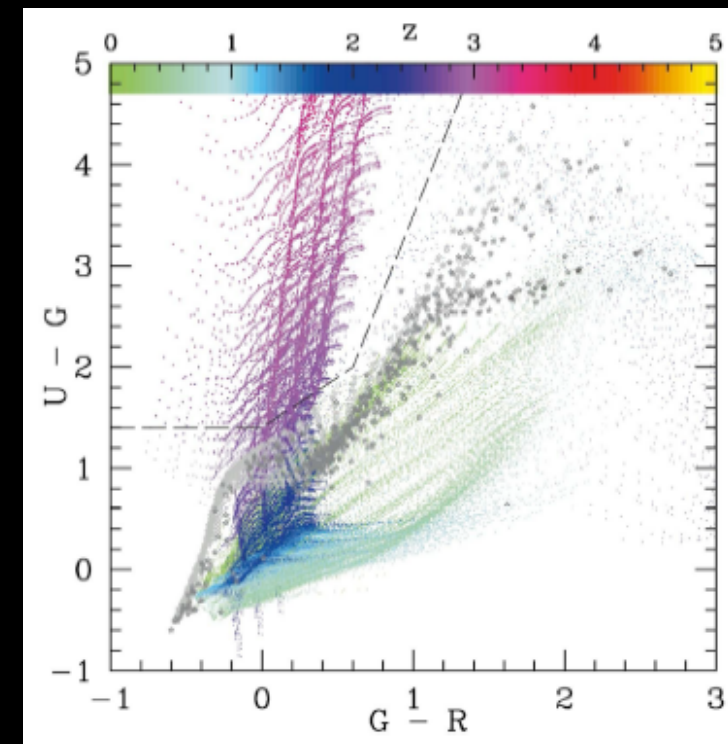
3000Å

4500Å

6060Å

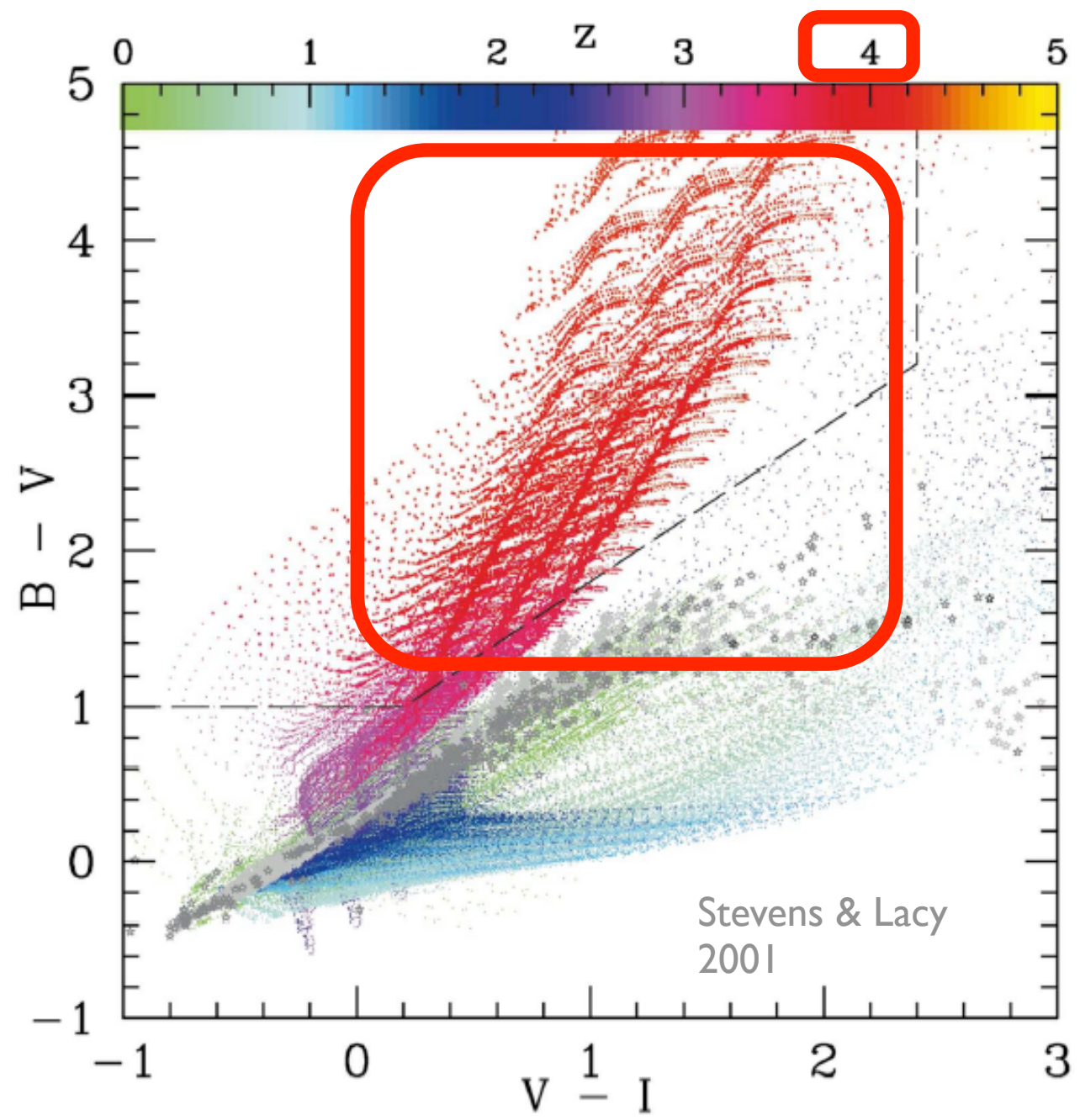
8140Å

# U-band dropouts in the Hubble Deep Field (HDF)



<http://www.astr.ua.edu/keel/galaxies/galevolve.html>

The panels show the brightest of the Lyman Break Galaxies above  $z=3$  in the original Hubble Deep Field, with wavelengths near 3000, 4500, 6060, and 8140 Å. The clumpy object in the center is comparably bright in the longer wavelengths, showing a flat spectrum, and vanished in the UV shortward of its Lyman break.

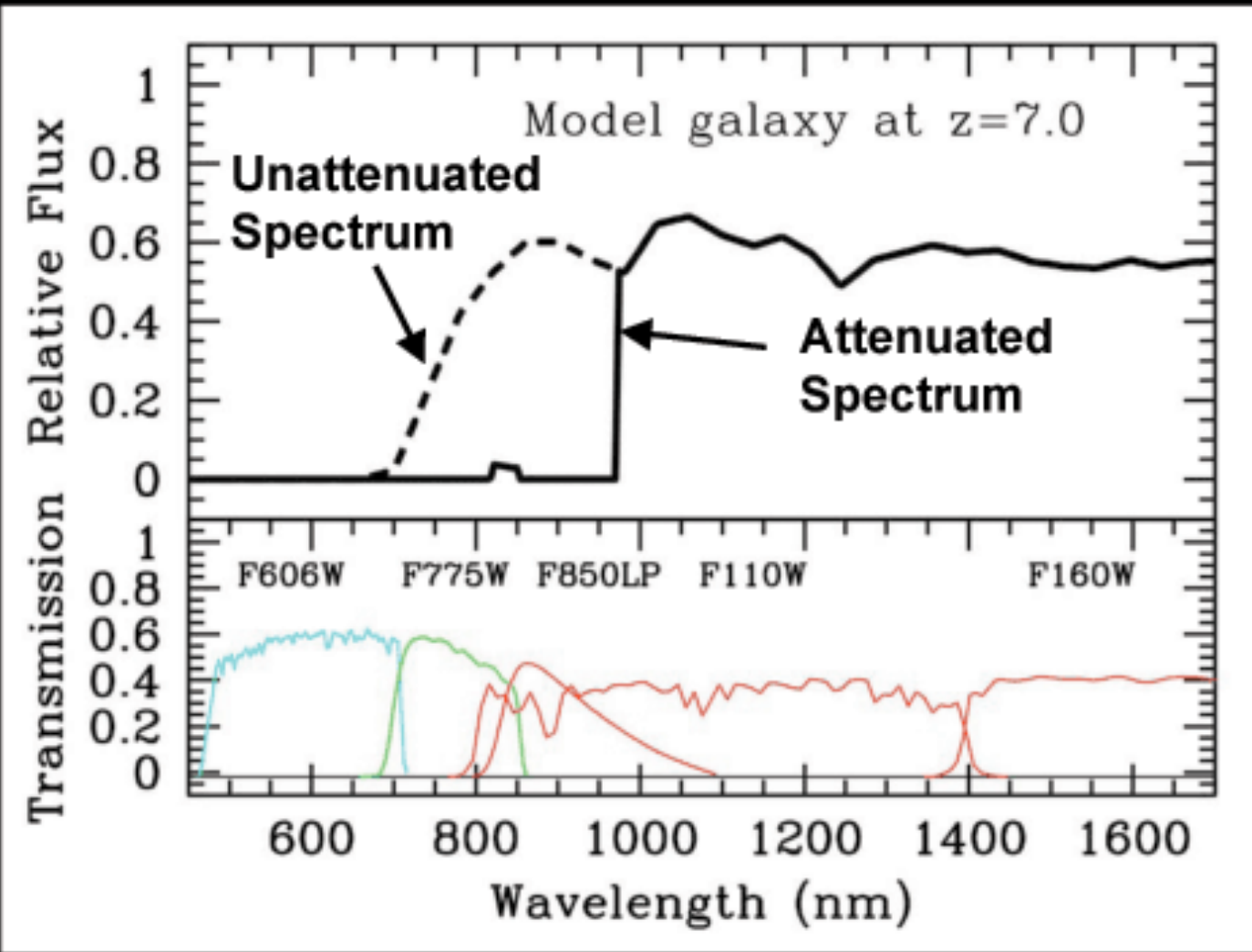


“B-band dropouts”, “V-band dropouts” etc, push to higher redshifts

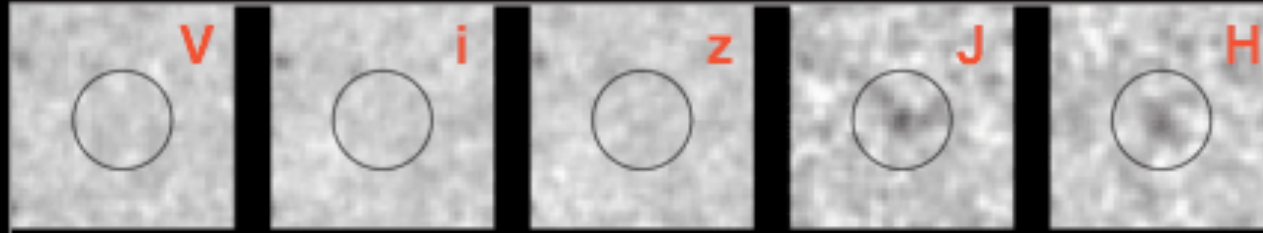
The general class of galaxies is known as “Lyman Break Galaxies”

Figure 8. As Fig. 5 but for  $B - V$  and  $V - I$ , and with galaxies in the redshift range  $3.5 < z < 4.5$  emphasized. Again there is good separation between the high-redshift galaxy population and the low-redshift galaxies and stars.

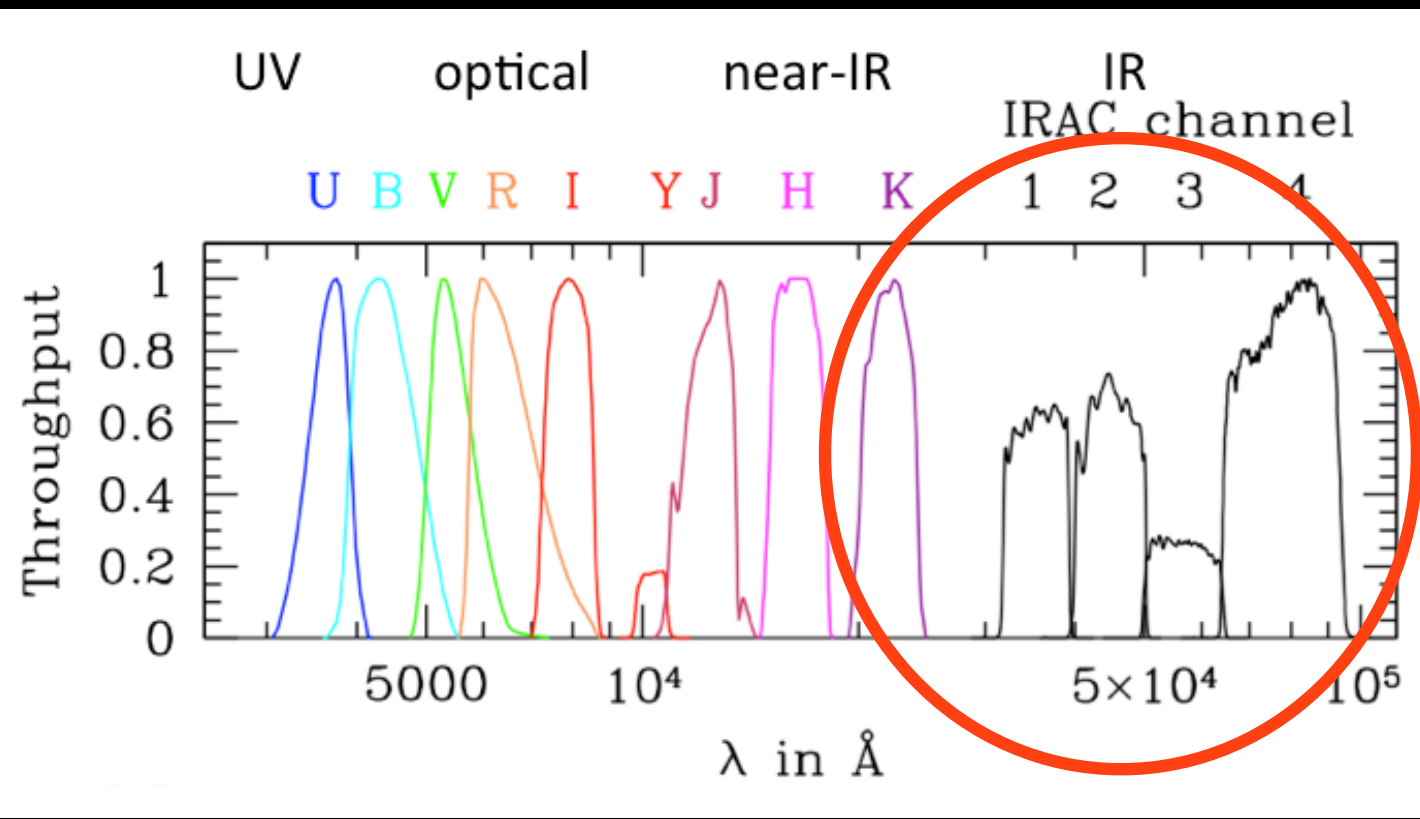
# State of the Art was optical dropouts



Only detected  
in deep HST  
imaging with  
WFC3/IR



# Current State of the Art: NIR dropouts



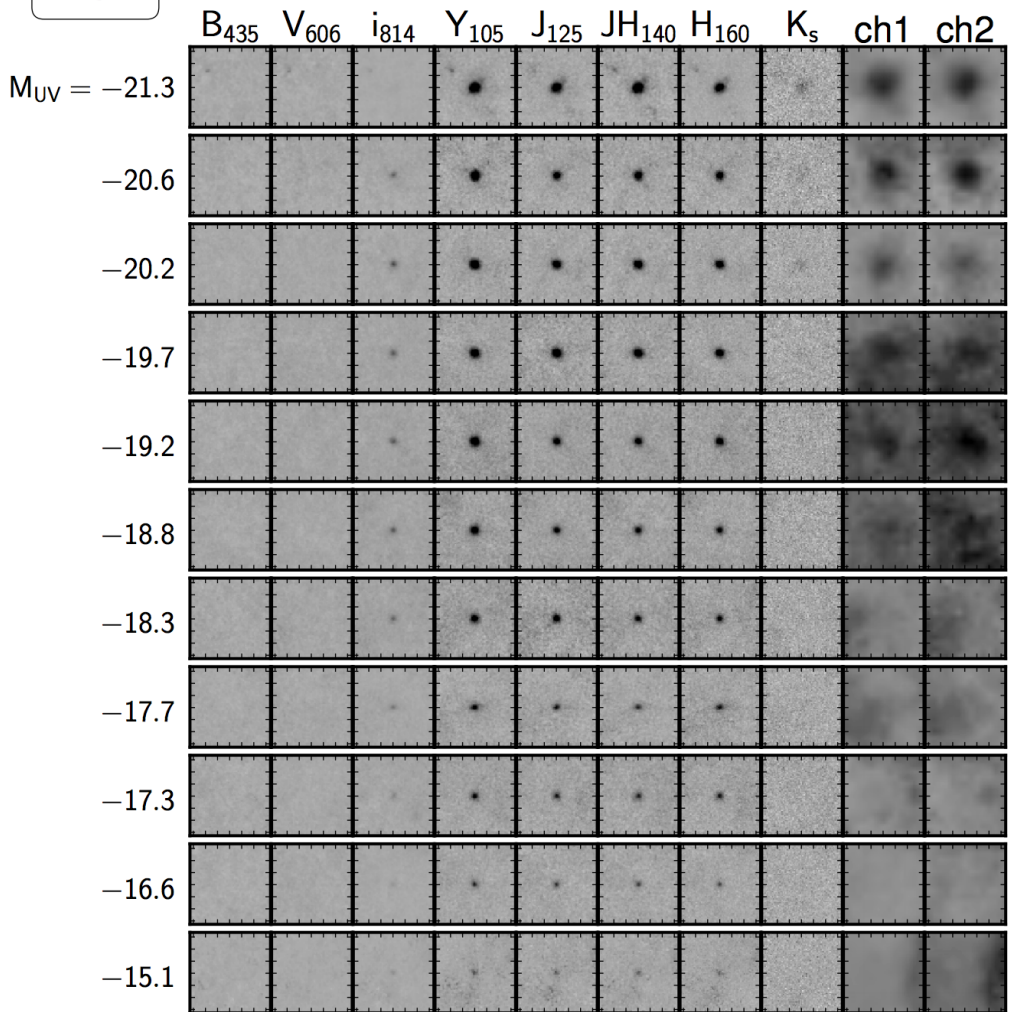
Invisible in  
deep HST  
imaging with  
WFC3/IR

Only seen in  
Spitzer and  
maybe  
ground-based  
K.

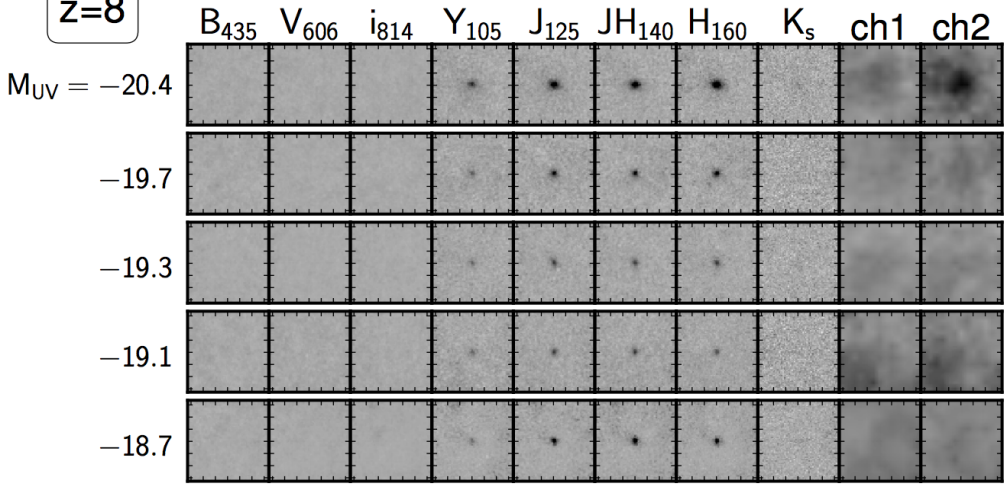
CANDELS: HST Multi-cycle  
HST Frontier Fields

# Example of highest-z identifications

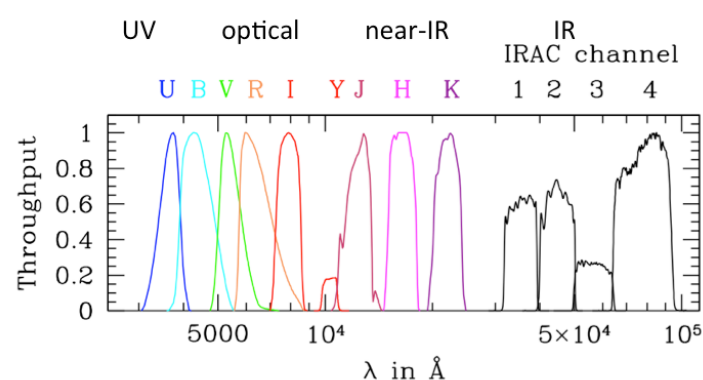
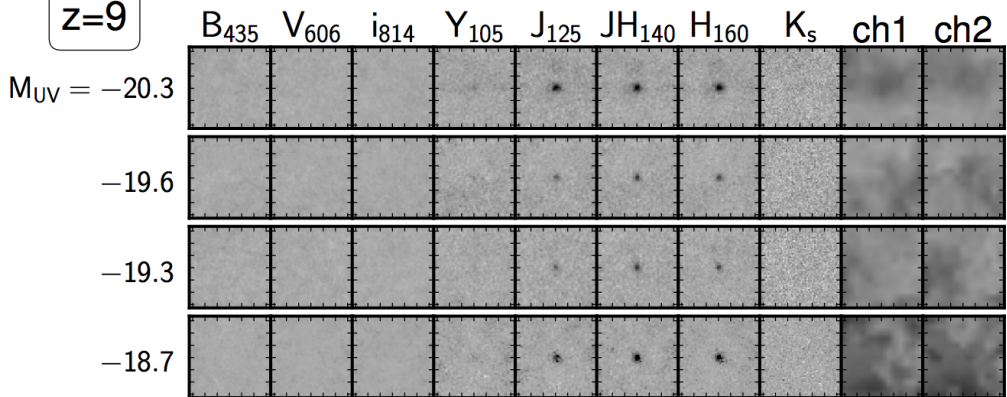
$z=6\text{-}7$



$z=8$

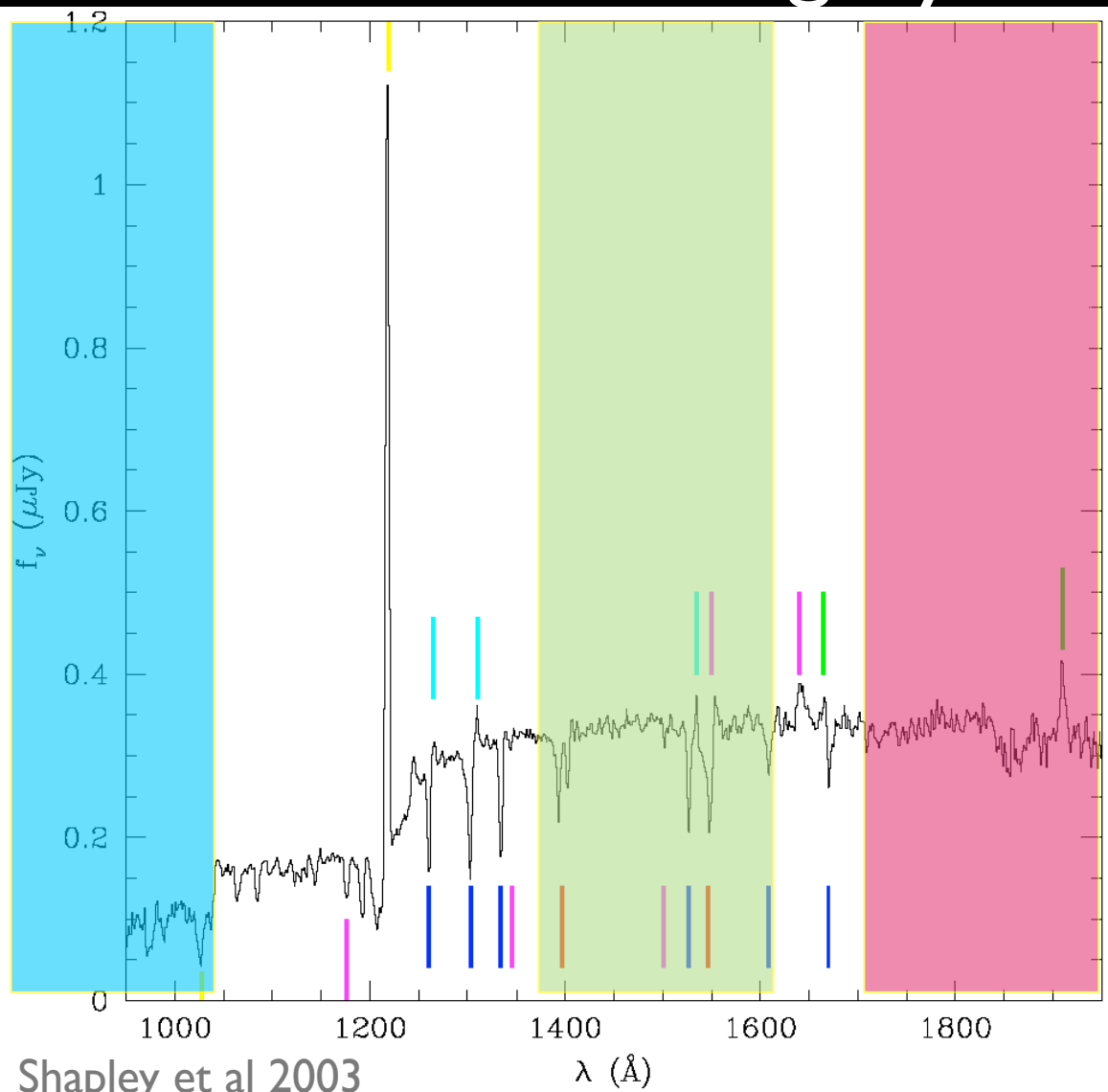


$z=9$



Kikuchihara et al 2019: Stacked photometry of drop outs in HST Frontier fields. HST+Keck+Spitzer IRAC 3.6, 4.5 $\mu$ m

# Important fact: All Lyman break galaxies are star forming, by construction



Shapley et al 2003

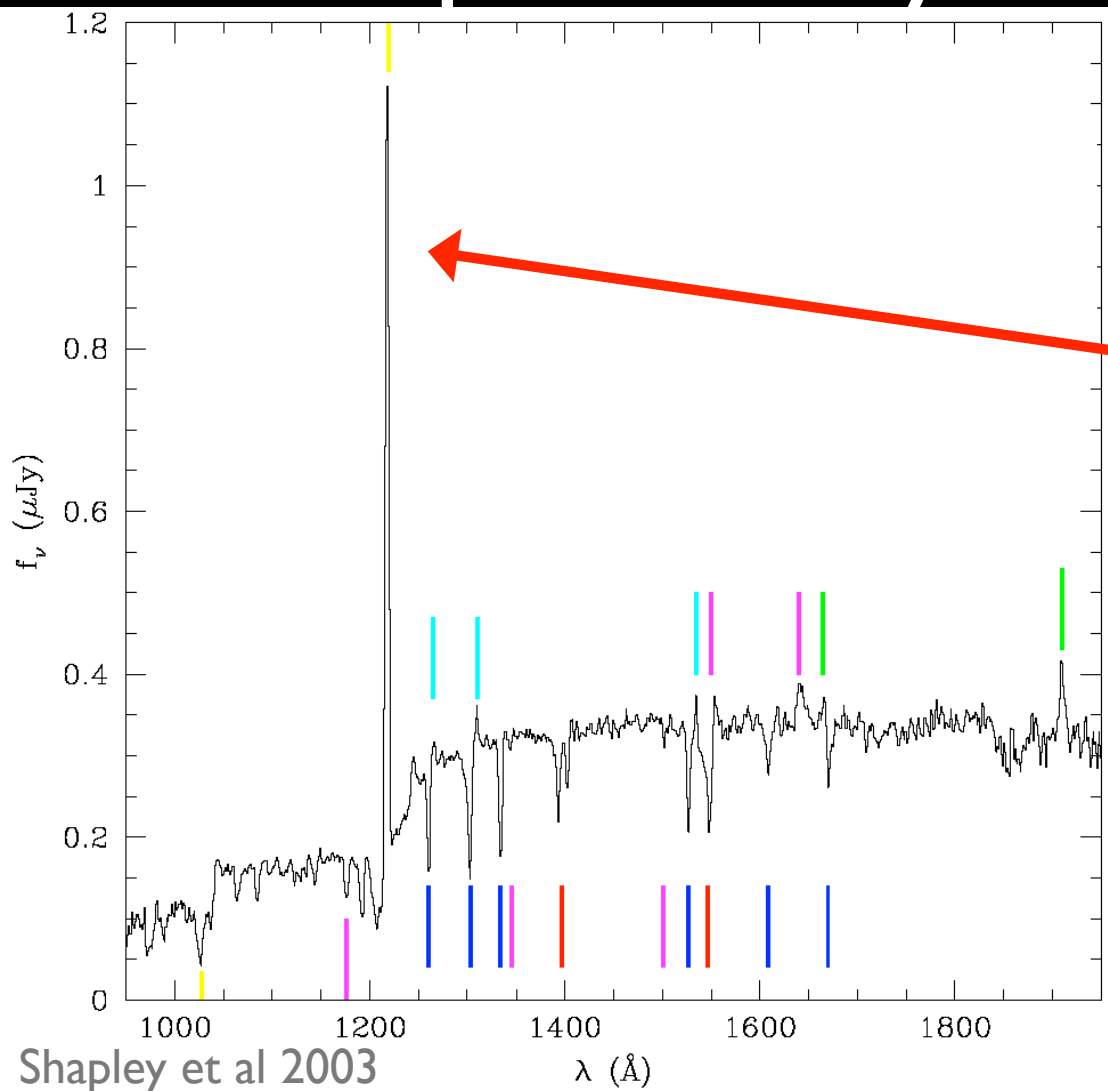
Significant UV flux  
(1300-2000Å)  
= O & B-stars

Rest-frame UV spectrum of  
coadded Lyman Break  
Galaxies (LBG) at  $z \sim 3$

Strong Ly $\alpha$  emission  
Blue trough shortward of  
Ly $\alpha$  = galactic-wide outflow?

FIG. 2.— A composite rest-frame UV spectrum constructed from 811 individual LBG spectra. Dominated by the emission from massive O and B stars, the overall shape of the UV continuum is modified shortward of Ly $\alpha$  by a decrement due to inter-galactic HI absorption. Several different sets of UV features are marked: stellar photospheric and wind, interstellar low- and high-ionization absorption, nebular emission from H II regions, Si II\* fine-structure emission whose origin is ambiguous, and emission and absorption due to interstellar HI (Ly $\alpha$  and Ly $\beta$ ). There are numerous weak features which are not marked, as well as several features bluewards of Ly $\alpha$  which only become visible by averaging over many sightlines through the IGM. The composite LBG spectrum is available in electronic form from <http://www.astro.caltech.edu/~aes/lbgspec/>.

# 4: Ly $\alpha$ Emitters: Selects SF galaxies, but potentially to lower SFRs

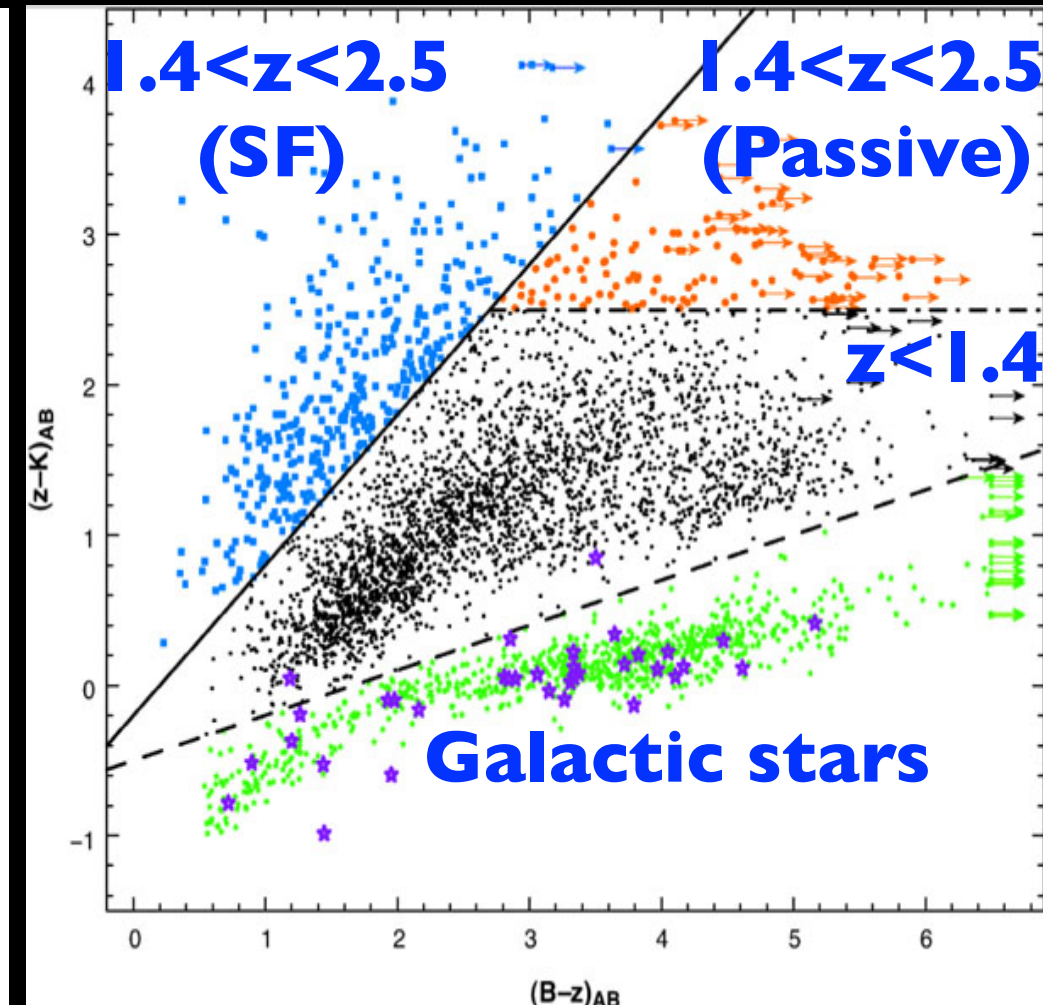
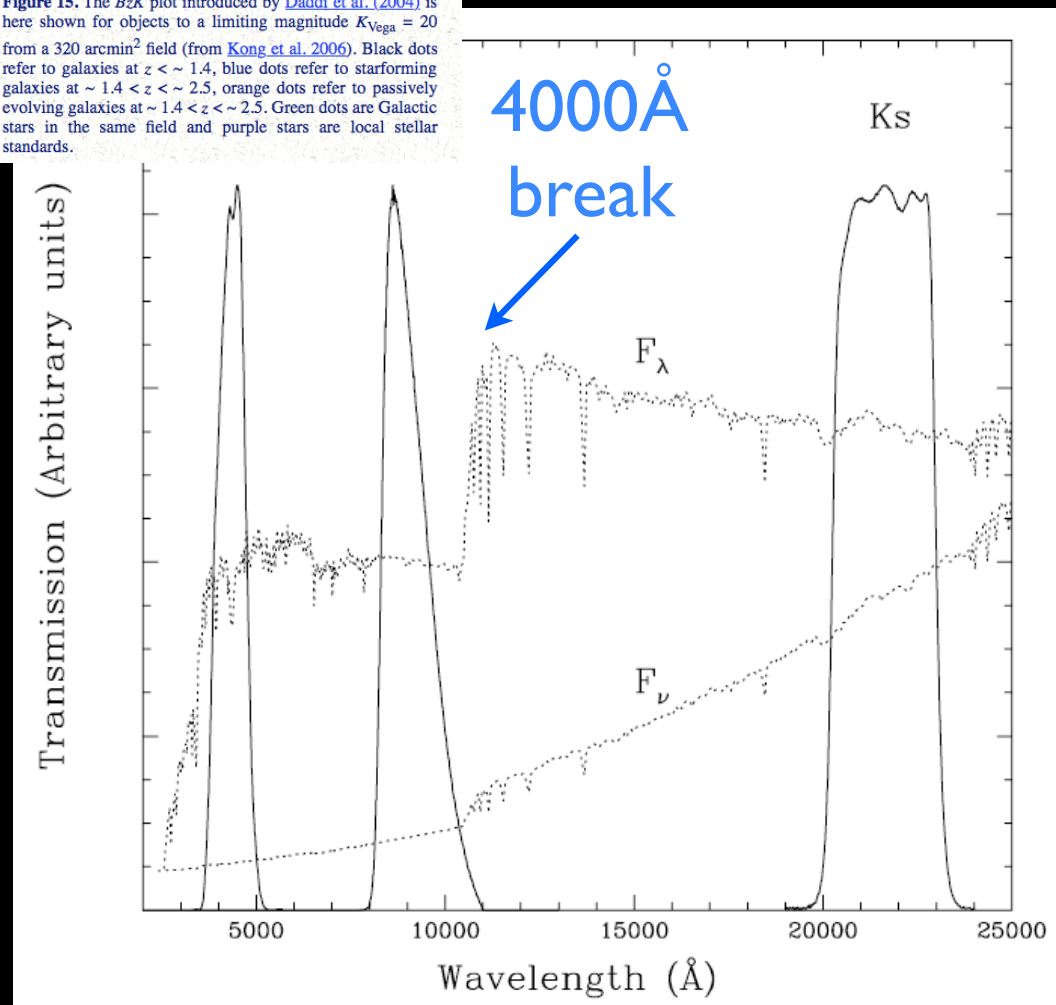


Select using  
narrow band  
filters targeting  
specific redshift

FIG. 2.— A composite rest-frame UV spectrum constructed from 811 individual LBG spectra. Dominated by the emission from massive O and B stars, the overall shape of the UV continuum is modified shortward of Ly $\alpha$  by a decrement due to inter-galactic HI absorption. Several different sets of UV features are marked: stellar photospheric and wind, interstellar low- and high-ionization absorption, nebular emission from H II regions, Si II\* fine-structure emission whose origin is ambiguous, and emission and absorption due to interstellar HI (Ly $\alpha$  and Ly $\beta$ ). There are numerous weak features which are not marked, as well as several features bluewards of Ly $\alpha$  which only become visible by averaging over many sightlines through the IGM. The composite LBG spectrum is available in electronic form from <http://www.astro.caltech.edu/~aes/lbgspec/>.

# 5.“BZK”: Selects for *both* star-forming or “passive” galaxies at high z

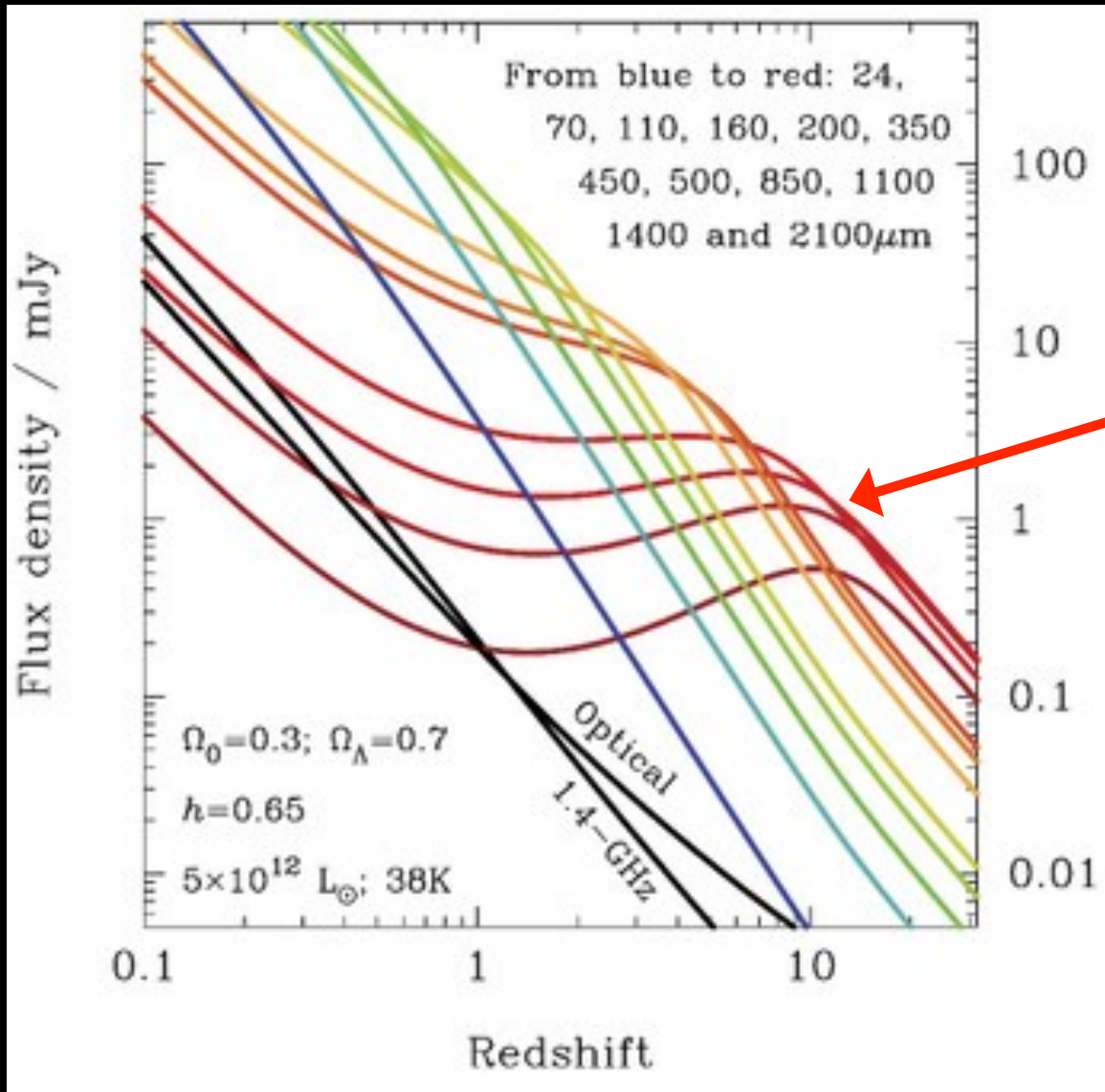
Figure 15. The  $BzK$  plot introduced by Daddi et al. (2004) is here shown for objects to a limiting magnitude  $K_{\text{Vega}} = 20$  from a 320 arcmin $^2$  field (from Kong et al. 2006). Black dots refer to galaxies at  $z < \sim 1.4$ , blue dots refer to starforming galaxies at  $\sim 1.4 < z < \sim 2.5$ , orange dots refer to passively evolving galaxies at  $\sim 1.4 < z < \sim 2.5$ . Green dots are Galactic stars in the same field and purple stars are local stellar standards.



Can detect non-SF galaxies, and obscured SF galaxies with high SFRs

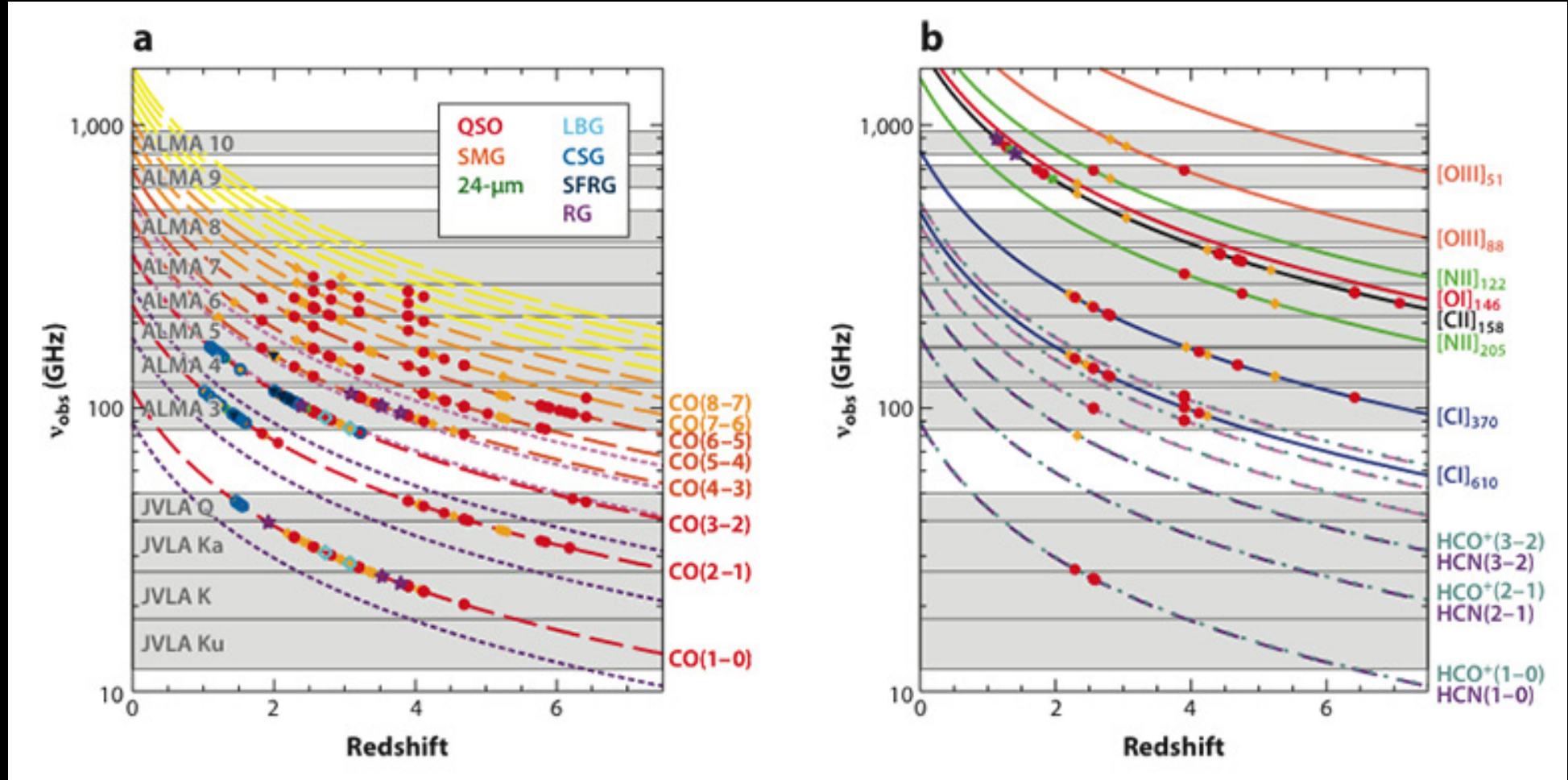
Introduced by  
Daddi et al 2004

# 6. Sub-mm observations (ALMA)

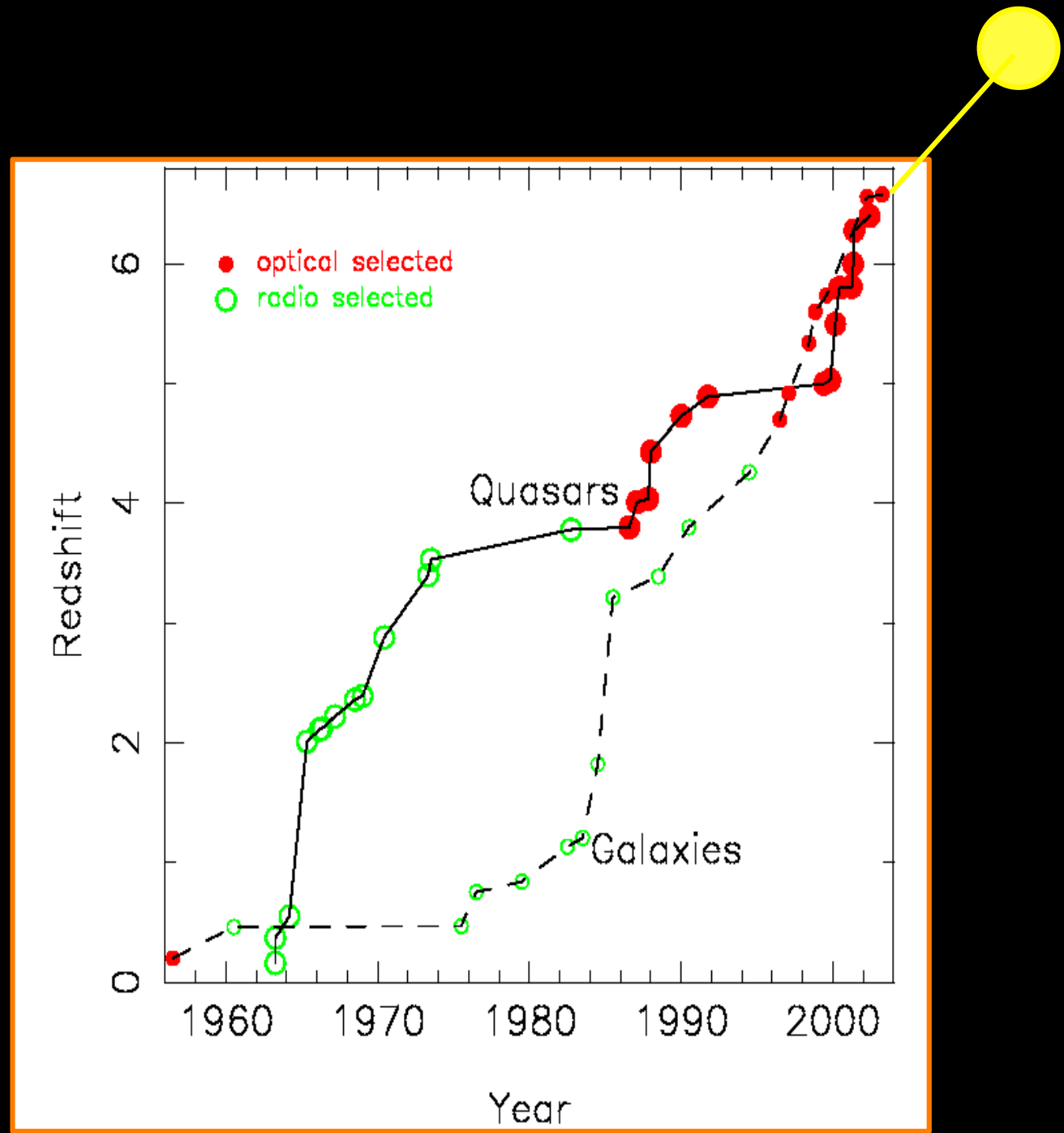


At long wavelengths, galaxies get *brighter* with increasing  $z$ , as cool dust peak moves into bandpass.

Note: Many lines available w/ ALMA at high spatial resolution, so good for kinematics and ISM physics of high-z galaxies



# Highest Redshift with Time



How do you measure evolution once  
you have identified galaxies at multiple  
redshifts?

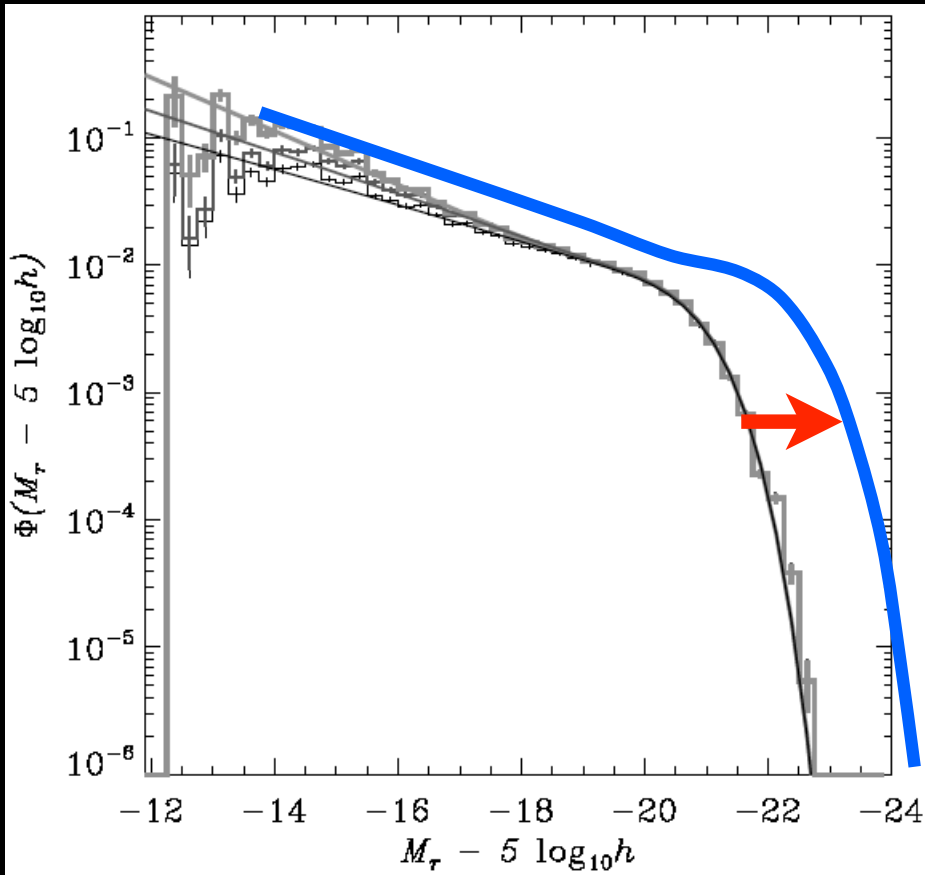
# 2 Main Strategies

- Broad population studies at a range of redshifts, by tracking 1 or more properties
  - Luminosity function evolution
  - Stellar mass function evolution
  - SFR evolution
  - SFR vs stellar mass evolution
- Tracking specific sub-populations through time
  - Red (“passive”) and blue (“sf”) sequences
  - Abundance matching

# A few technical points before results:

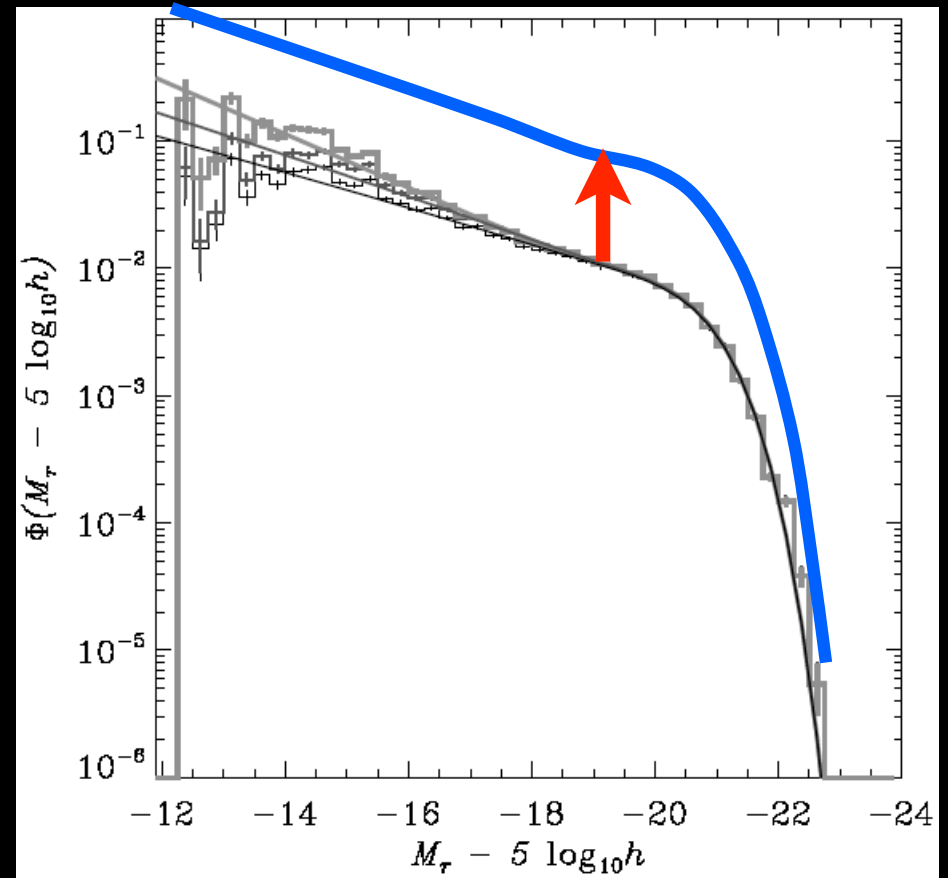
1. Types of Evolution
2. Separating star forming and “passive” galaxies
3. Abundance matching techniques

# I. Two broad classes of evolution



Luminosity Evolution:

All galaxies brighter

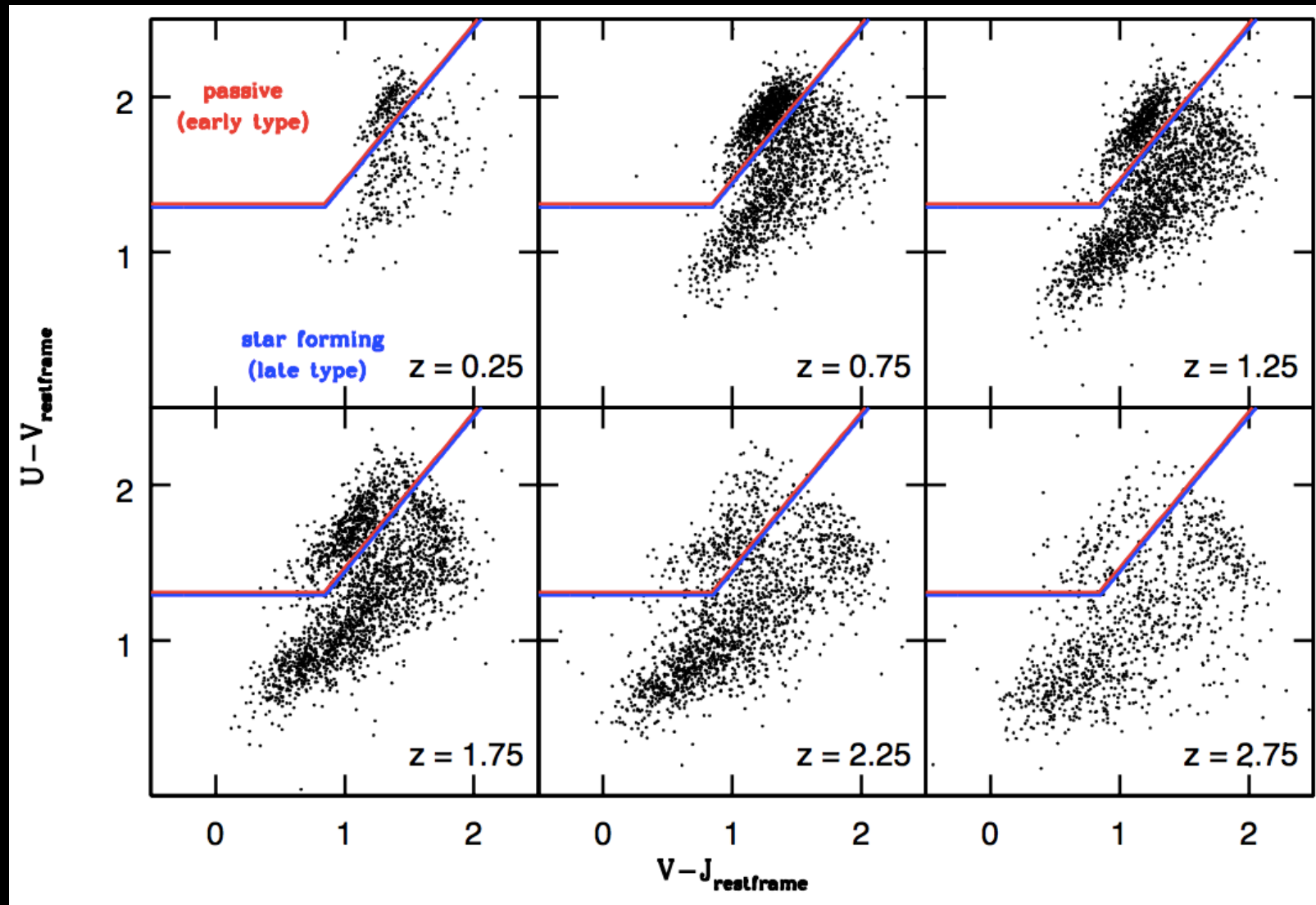


Density Evolution:

More galaxies at each luminosity

Reality? Far more complex

## 2. Separating SF from Passive galaxies



van der Wel et al 2014

Use bimodality w/ appropriate color cuts, being careful about dust

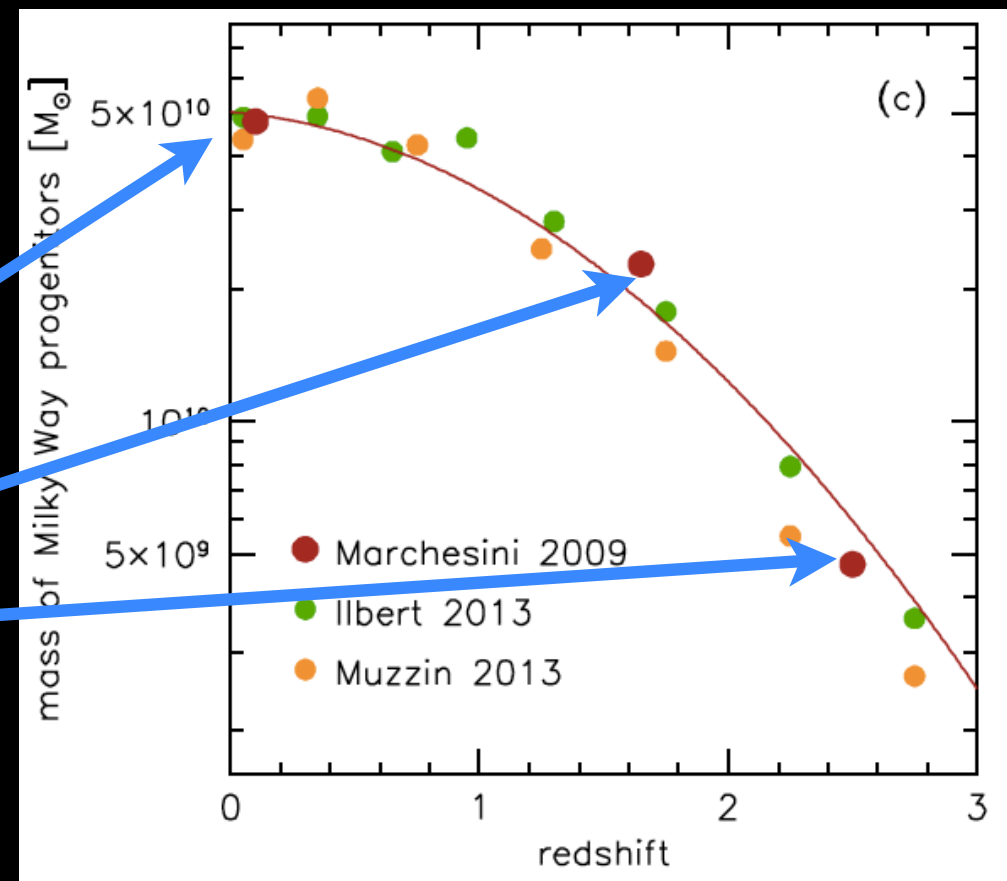
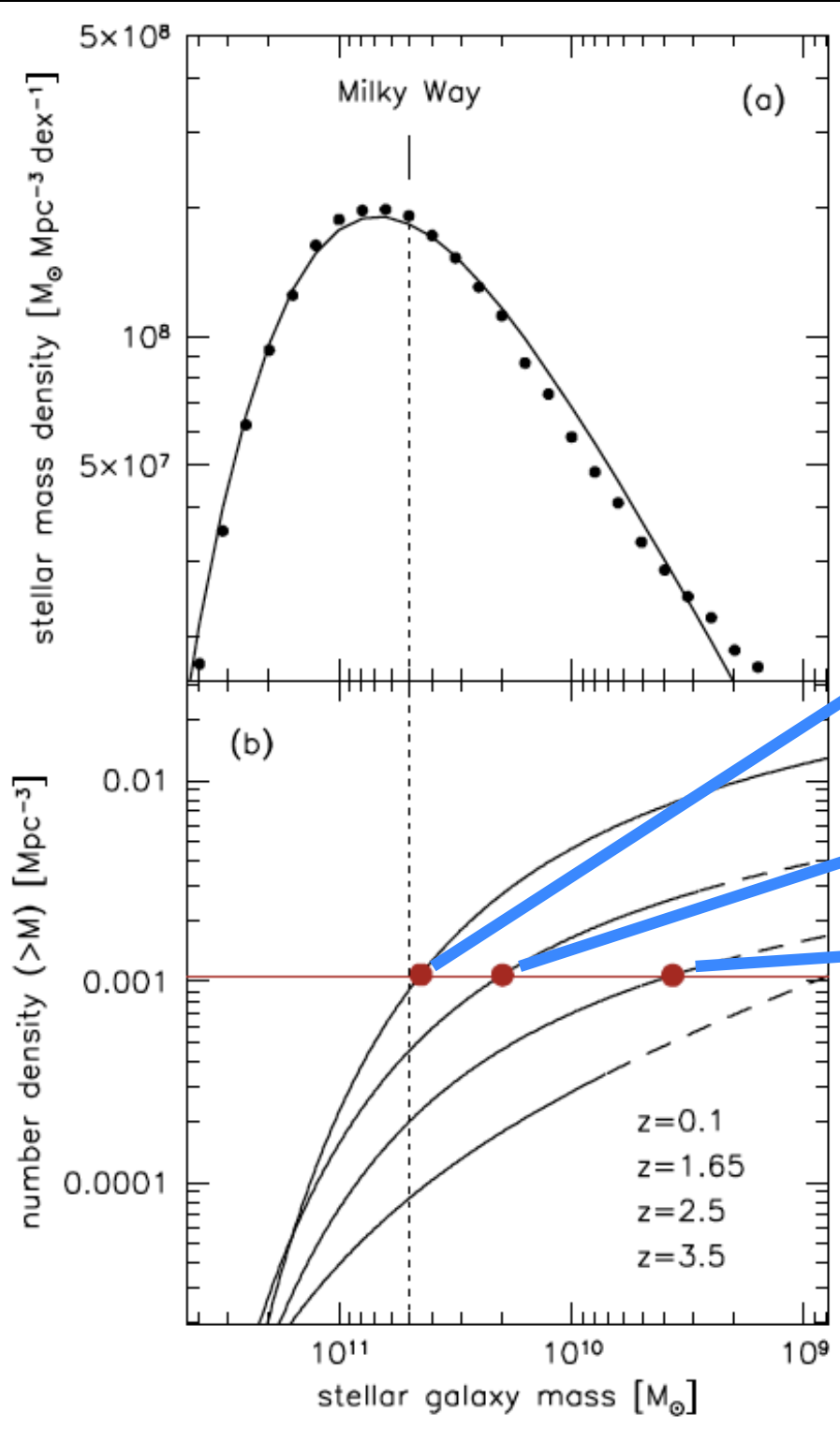
# 3. Matching galaxies across cosmic time

- Abundance matching
  - Assume brightest galaxies at each redshift live in the most massive halos (gives  $M_{\text{star}}$  vs  $M_{\text{halo}}$ )
- “Halo Occupation Distributions”
  - Match samples with identical correlation properties at each redshift

(i.e., which galaxies at  $z>1$  are progenitors of MW? of giant ellipticals, etc?)

Assumes rank order is conserved, or that breaking rank is unimportant on average

# Example for MW progenitors



# Abundance Matched MW Progenitors

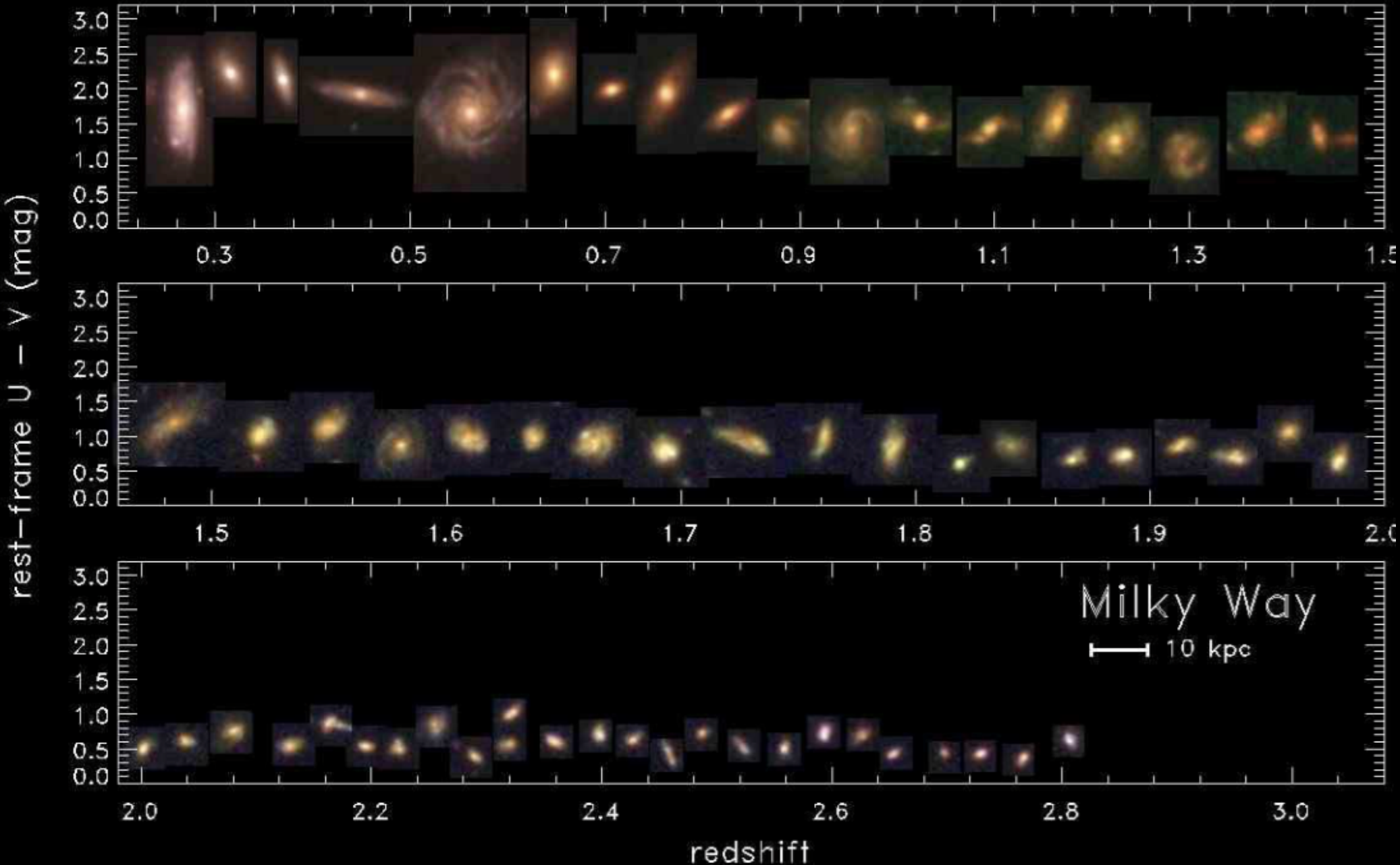
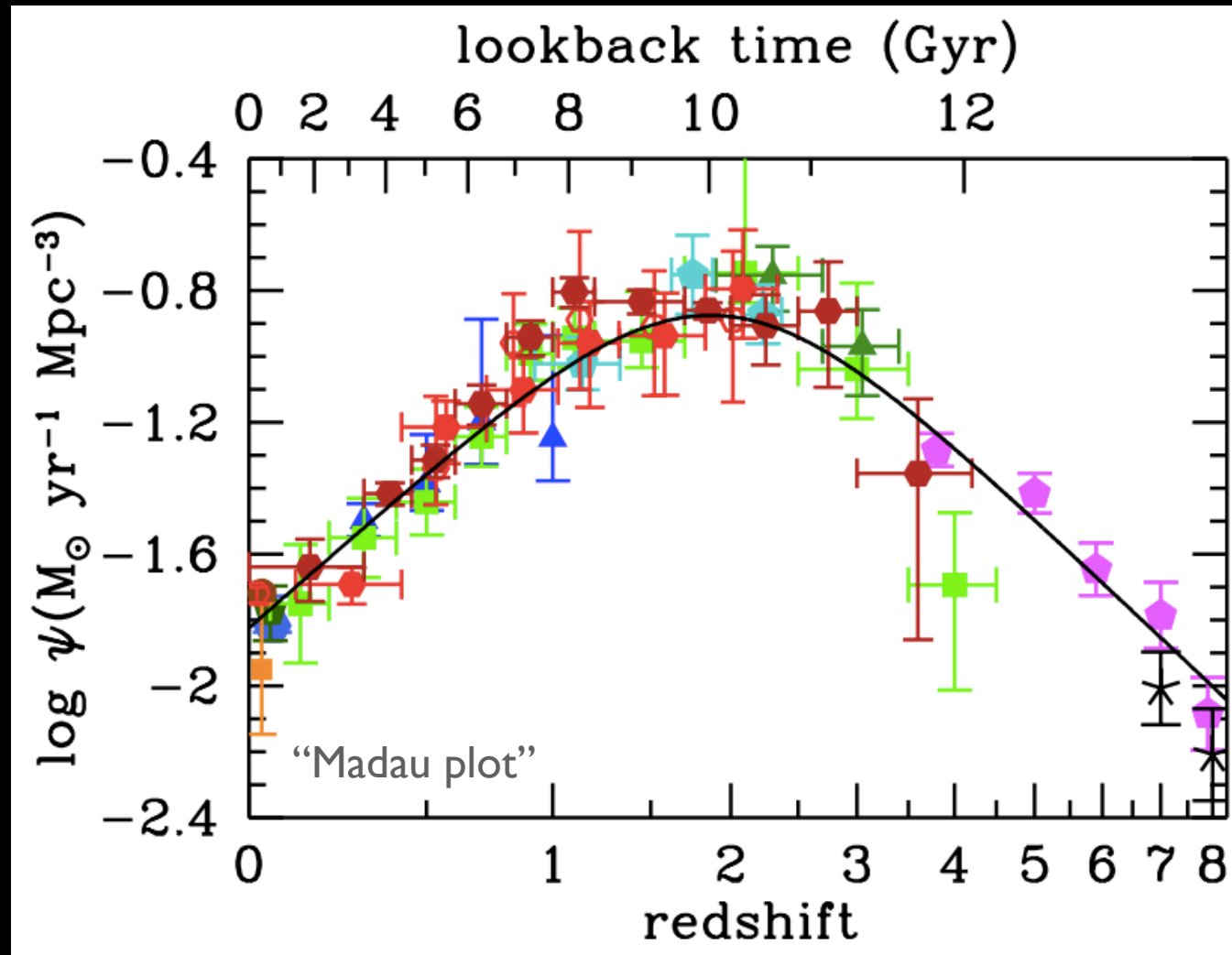


**Figure 12.** Examples of progenitors of an M31-mass galaxy from  $z = 3$  to the  $z = 0.5$ . Each galaxy is selected such that it has the (approximate) median  $U - V$  and  $V - I$  color derived for all progenitors in a given redshift bin (see Table 1). Each false-color image shows the approximate rest-frame  $U$ ,  $B$ ,  $V$ -band (blue, green, red, respectively) using the ACS ( $B_{435}V_{606}F_{752850}$ ) and WFC3 ( $J_{125}H_{160}$ ) band closest to rest-frame  $UVB$  at each redshift (for this reason we show only progenitors from the CDF-S sample, because this full complement of *HST* imaging does not exist for the COSMOS nor UDS ZFOURGE fields, see Grogan et al. 2011; Koekemoer et al. 2011). The images are placed at their measured rest-frame  $U - V$  color and redshift (slight adjustments in redshift are made for presentation purposes, but the rank order of the galaxies is unchanged). The image sizes are scaled to the same fixed physical scale where the inset shows a scale of 10 kpc.

Papovich et al 2015

# Highlights of evolution studies

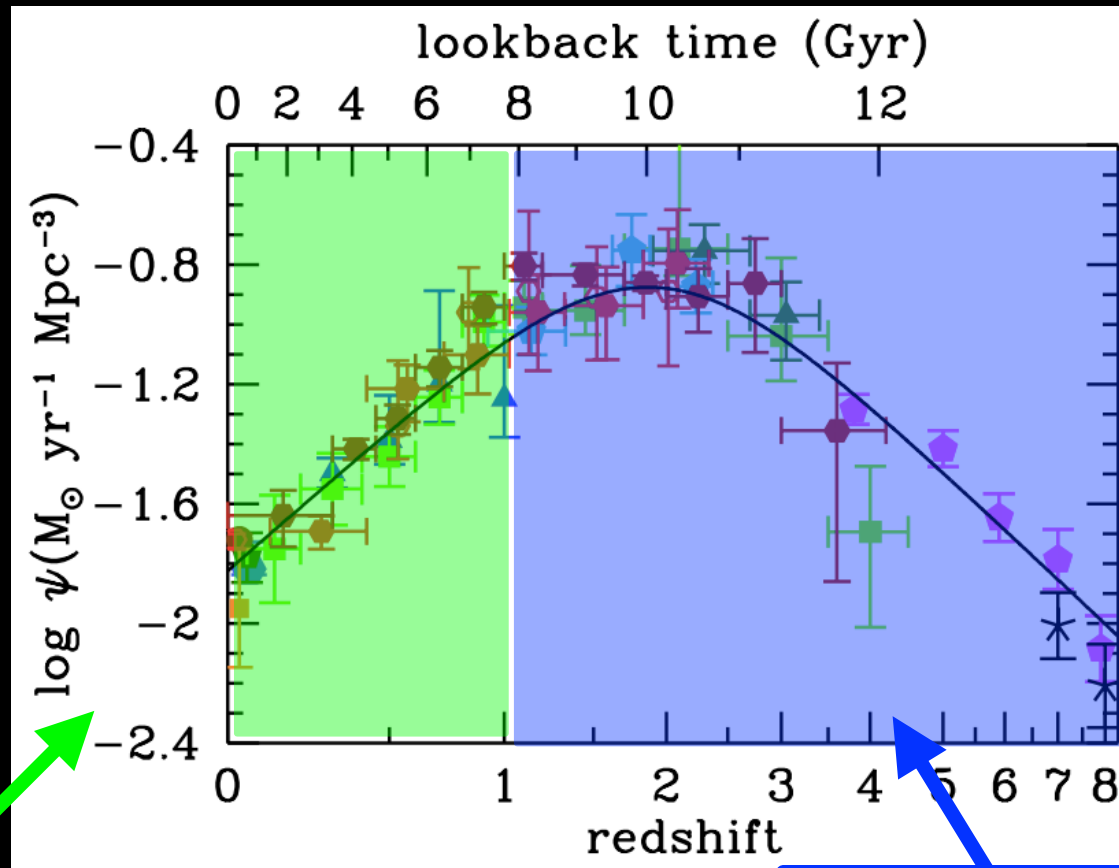
# I. Star formation rate peaked sometime around z=2-ish



Madau & Dickinson ARAA 2014

- Lots of uncertainties in extinction corrections, conversion to SFR, etc

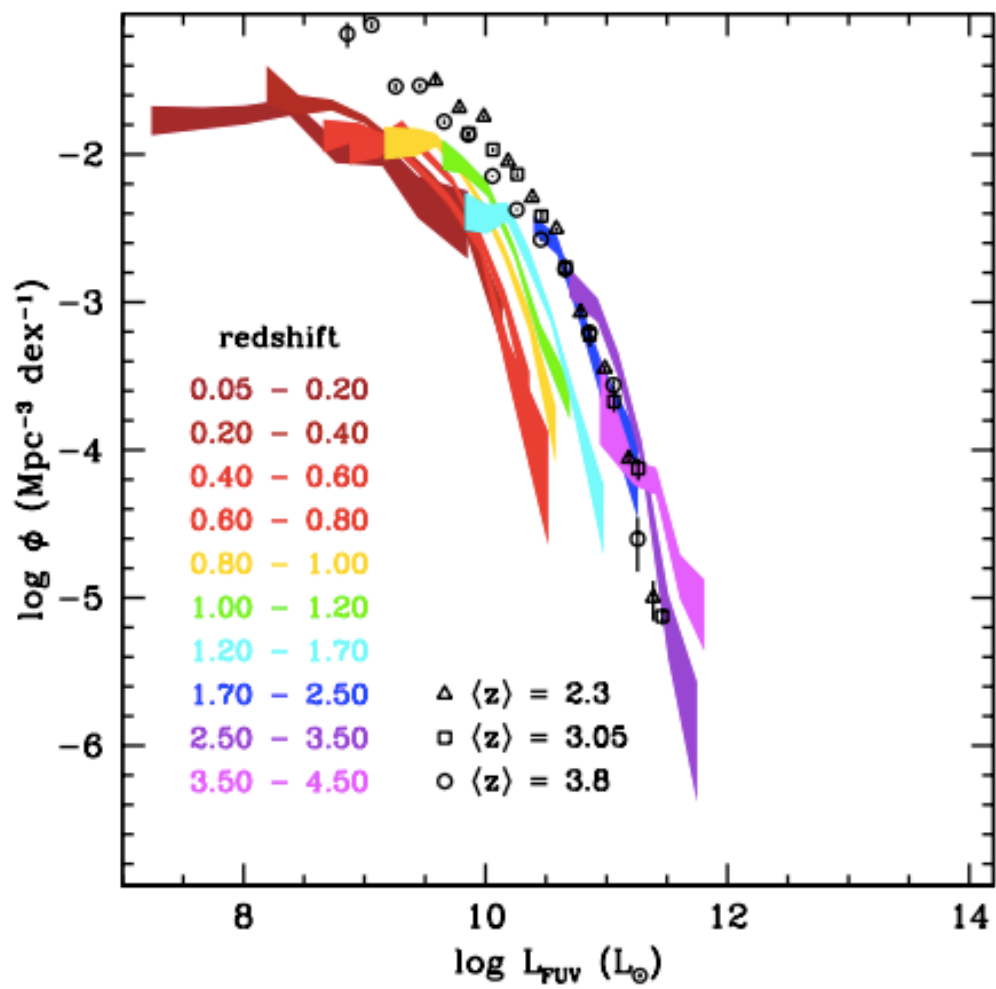
# I. Star formation rate peaked sometime around z=2-ish



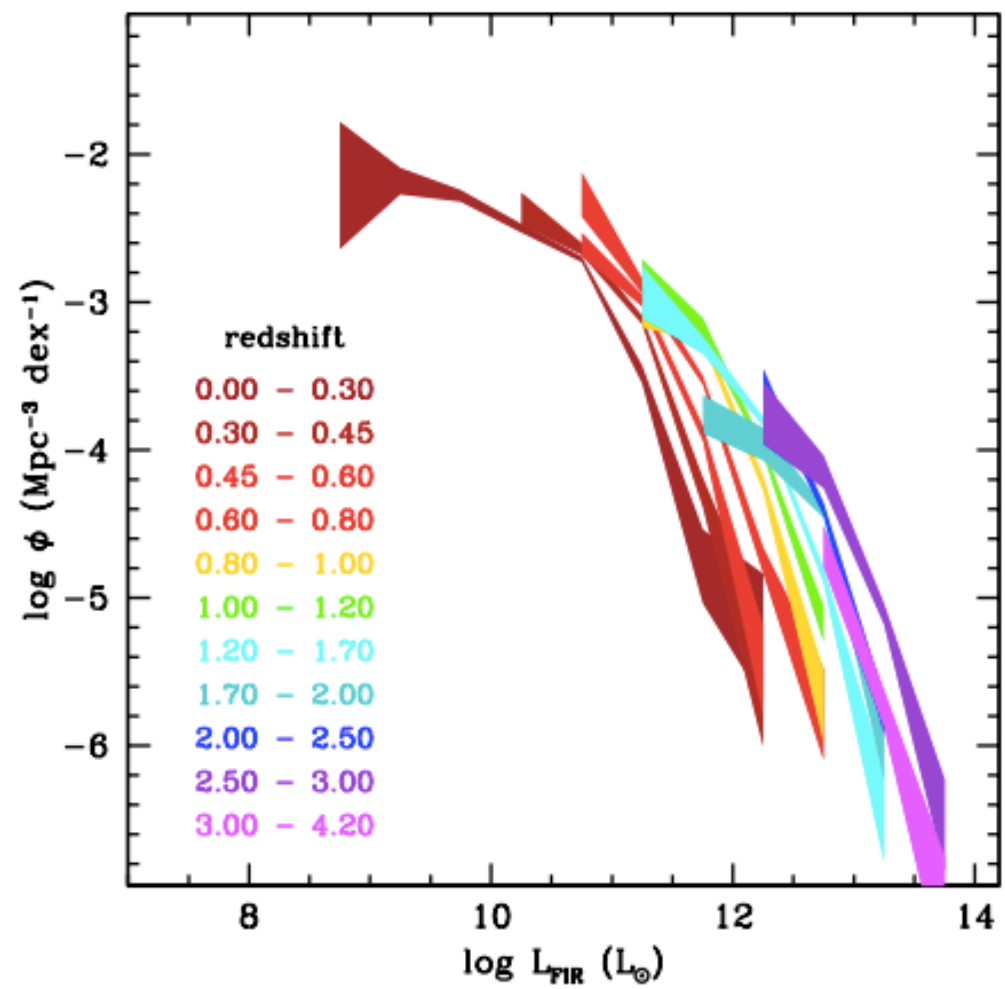
Late epoch of more quiescent evolution of disks & bulges

Initial epoch of rapid merging  
Mimics DM merging rates

# Ia. Associated with rapid evolution of UV and FIR luminosity



FUV Luminosity function



FIR Luminosity function

## 2. Galaxy density evolves rapidly at early times

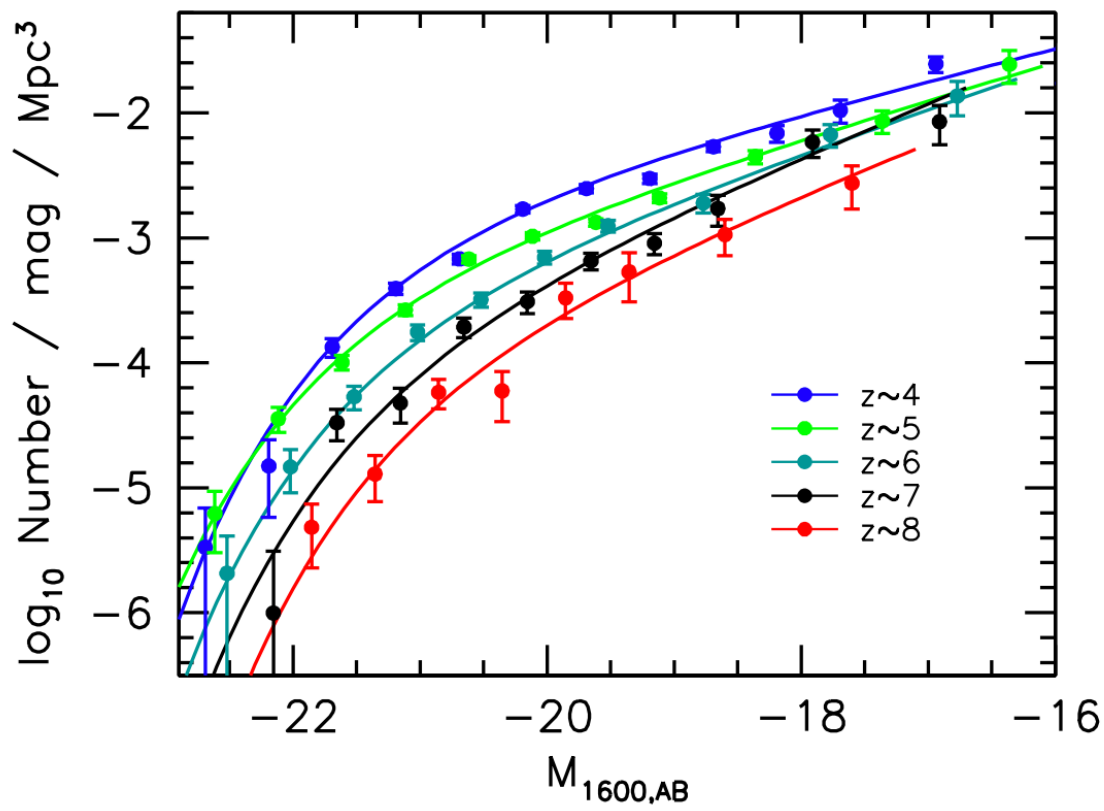
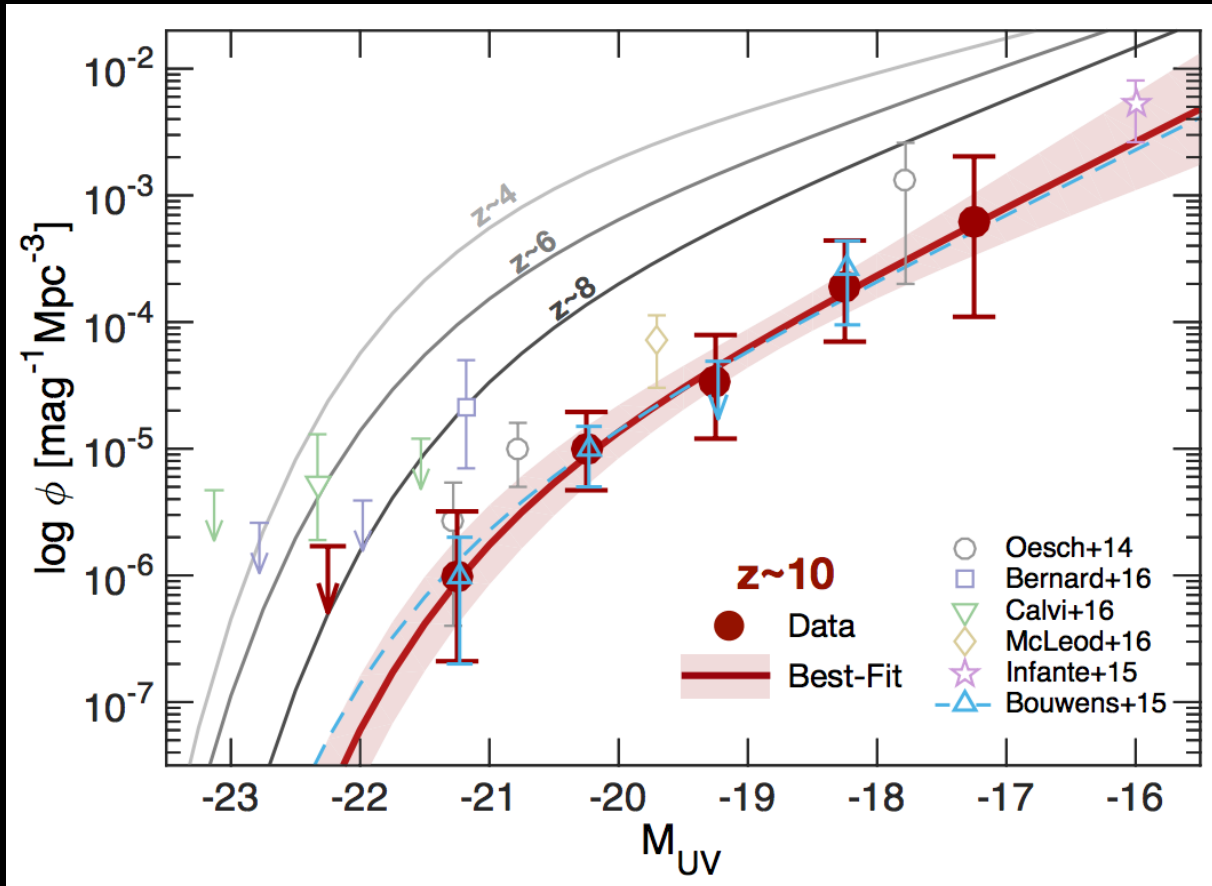


FIG. 6.— SWML determinations of the UV LFs at  $z \sim 4$  (blue solid circles),  $z \sim 5$  (green solid circles),  $z \sim 6$  (light blue solid circles),  $z \sim 7$  (black circles), and  $z \sim 8$  (red solid circles). Also shown are independently-derived Schechter fits to the LFs using the STY procedure (see §4.2). The UV LFs we have derived from the complete CANDELS+ERS+XDF+HUDF09 data sets show clear evidence for the build-up of galaxies from  $z \sim 8$  to  $z \sim 4$ . Note the appreciable numbers of luminous galaxies at  $z \sim 6$ ,  $z \sim 7$  and  $z \sim 8$ .  
Bouwens et al 2015

Number density increases with time, and faint-end slopes becomes shallower.

All based on very deep HST observations w/ photometric redshifts (mostly dropout constraints)

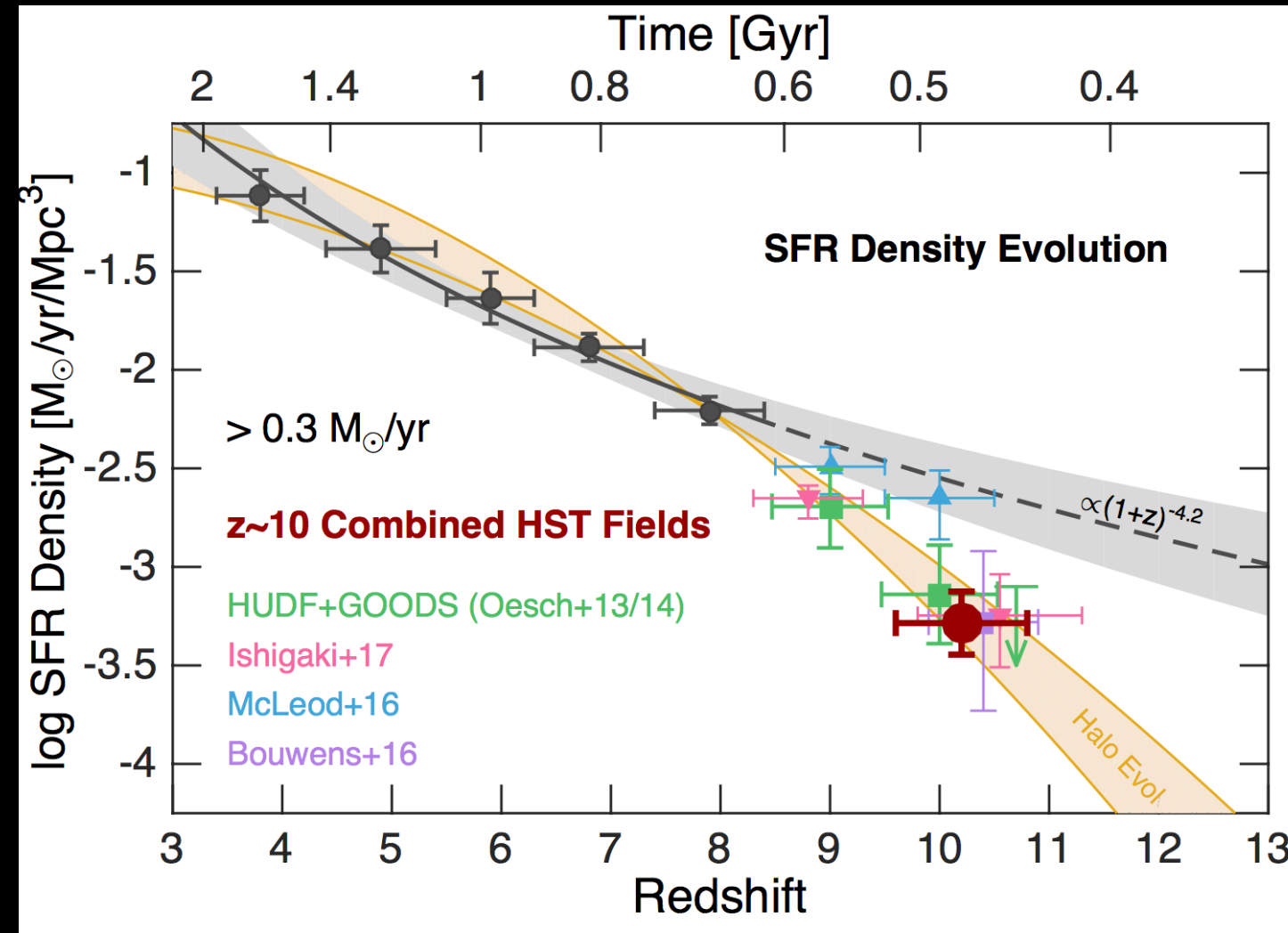
## 2. Galaxy density evolves rapidly at early times



Studies of lensed galaxies behind galaxy clusters do not find as many  $z \sim 10$  galaxies as expected

FIG. 2.— The measured UV LF at  $z \sim 10$ . The red points with errorbars correspond to our new measurements from all the *HST* legacy datasets. The red solid line is our best-fit LF with  $1\sigma$  uncertainty contours. These new results can be compared to previous measurements based on a subset of these datasets from Oesch et al. (2014) (gray open circles) and the independent analysis from Bouwens et al. (2015) (dashed blue line and open triangles). Given the overlap in datasets (5 of the 9 candidates are from the older datasets), the excellent agreement with the latter is not entirely surprising, but it is nevertheless encouraging. The new measurements confirm our previous results and show again that the UV LF evolves very rapidly at  $z > 8$ . Some previous analyses resulted in higher values for the UV LF, however, which include the BORG analyses from Bernard et al. (2016) and Calvi et al. (2016), as well as the HFF+CLASH analysis from McLeod et al. (2016). This is discussed more extensively in Section 4.1.2.

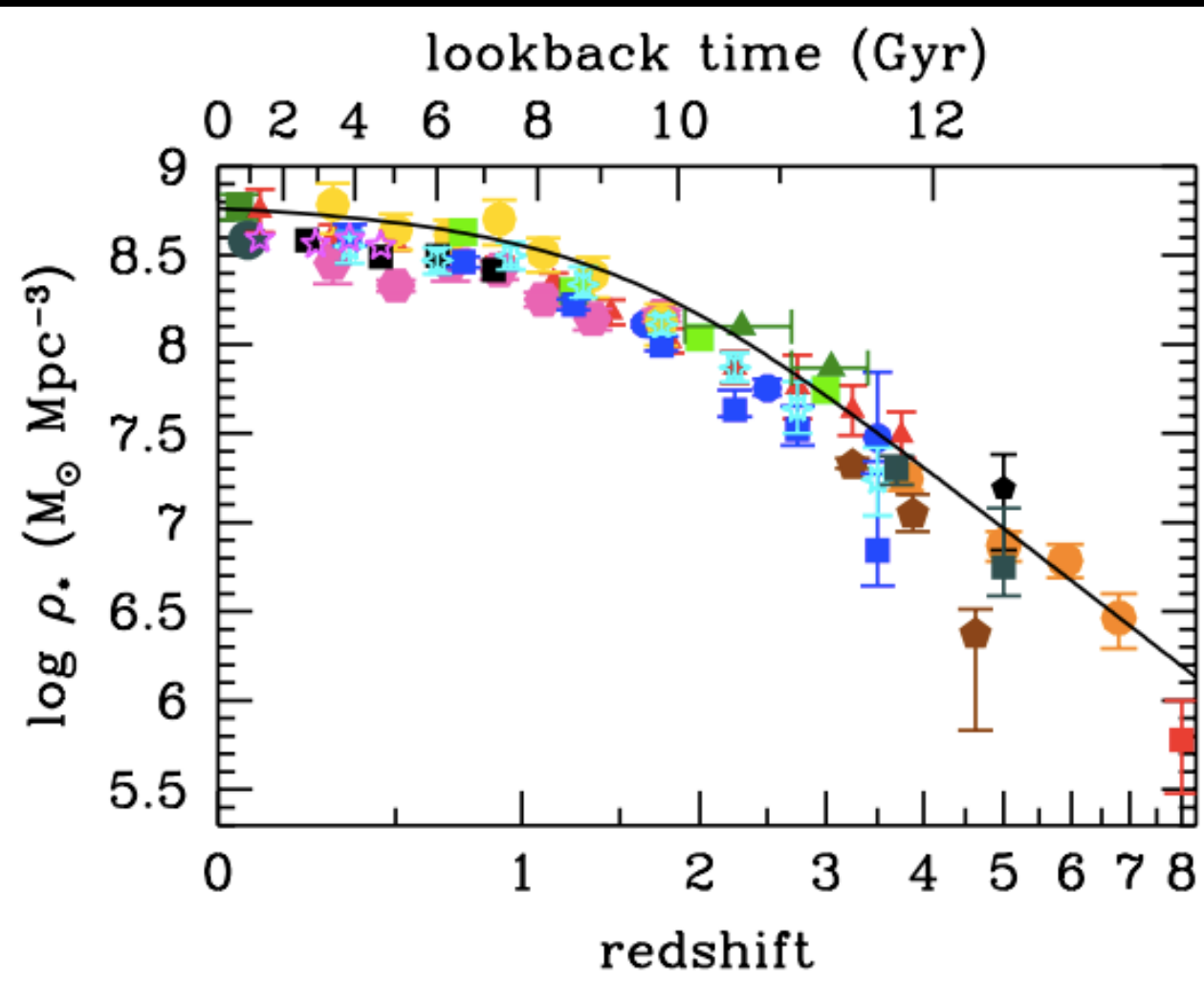
## 2. Galaxy density evolves rapidly at early times



$z=8-10$  evolution  
is extremely rapid,  
and follows  
growth of DM  
halo mass  
function

FIG. 5.— The evolution of the cosmic SFR density at high redshift integrated down to a UV luminosity of  $M_{UV} = -17.0$  (SFR  $> 0.3 M_{\odot} \text{ yr}^{-1}$ ). Lower redshift measurements (gray dots) have been updated from ALMA constraints in Bouwens et al. (2016a) assuming an evolving dust temperature and they include a small contribution from ULIRGS. Also shown are the measurements from Ishigaki et al. (2015, pink triangle) and McLeod et al. (2016, blue triangles), which have been corrected to our integration limit and UV luminosity to SFR conversion factor. The new measurement from the combination of all *HST* fields (filled dark red circle) confirms the rapid, accelerated evolution of the SFRD between  $z \sim 8$  to  $z \sim 10$ , as has previously been found in the HUDF+GOODS fields (Oesch et al. 2014; Bouwens et al. 2015). The evolution is significantly faster than at lower redshift (gray shaded region), which is not unexpected given the fast evolution of the halo mass function over this redshift range (see Sect 4.4). To illustrate this, the orange shaded region shows the relative evolution of the cumulative DM halo mass function integrated down to  $\log M_h/M_{\odot} = 9.5 - 10.5$  and normalized at the  $z \sim 8$  SFRD value. Clearly the evolution of the DM halos is in very good agreement with the substantial decrease in the SFRD at  $z > 8$ .

### 3. Stellar Mass of Universe has doubled since $z \sim 1-1.5$



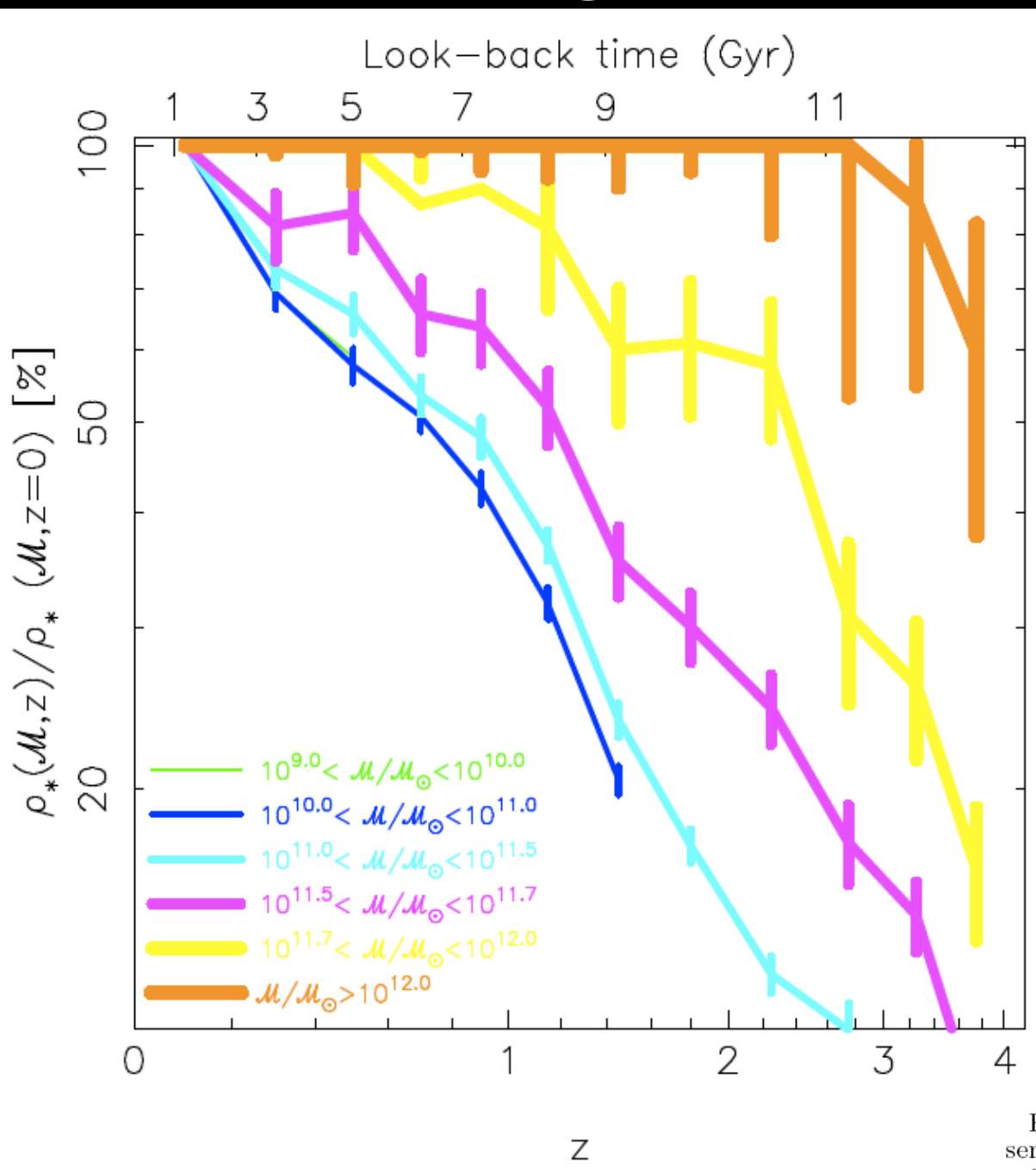
Integrated SFR  
predicts somewhat  
more stellar mass  
today than we see

But, lots of possible  
sources of bias

Madau & Dickinson ARAA 2014

Figure 11: The evolution of the stellar mass density. The data points with symbols are given in Table 2. The solid line shows the global stellar mass density obtained by integrating the best-fit instantaneous star-formation rate density  $\psi(z)$  (Equations 2 and 15) with a return fraction  $R = 0.27$ .

# 4. Massive galaxies finished SF earlier

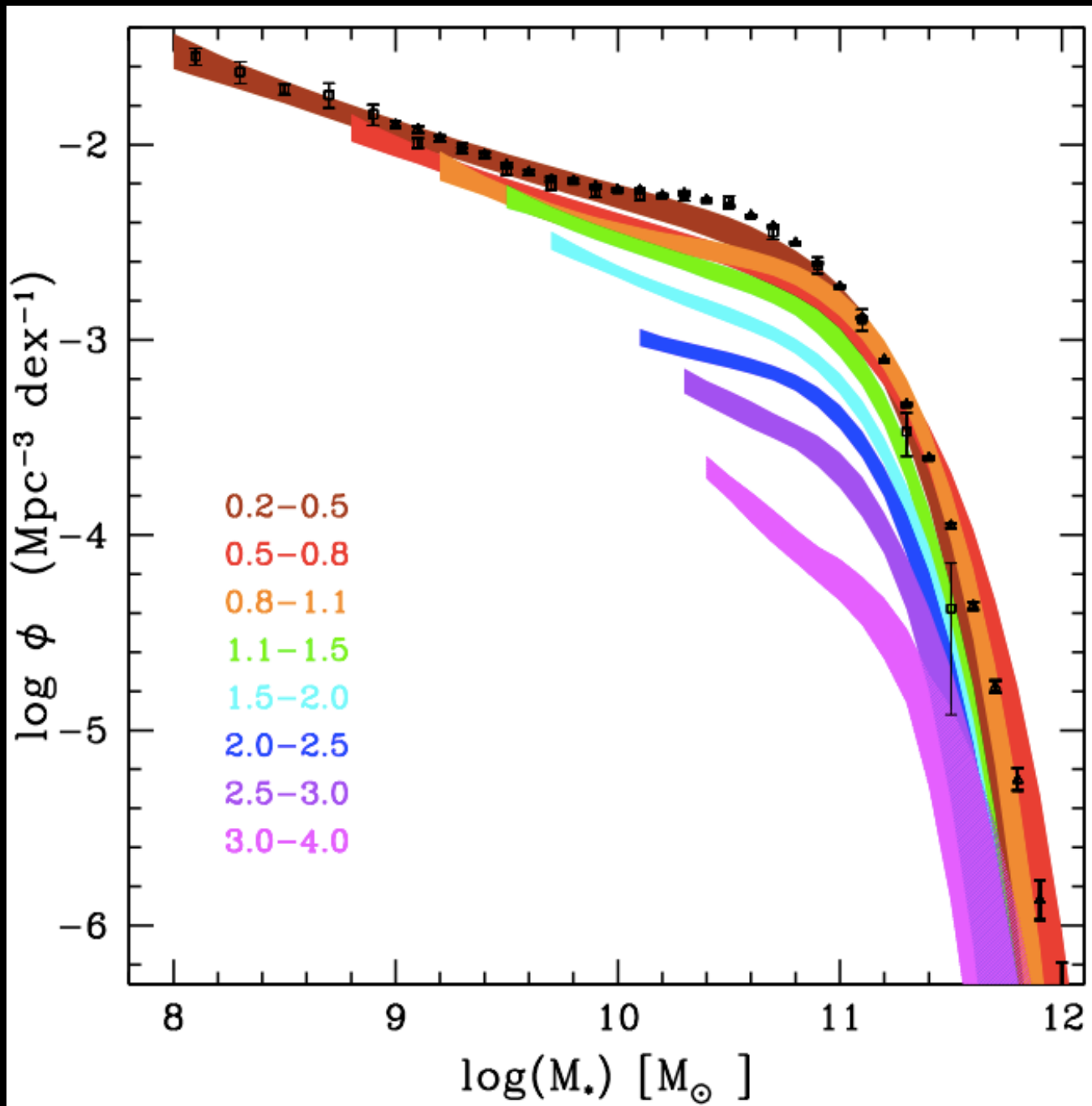


Largely in  
place by  $z=2$

Perez-Gonzalez et al 2008

FIG. 6.— Fraction of the local stellar mass density already assembled at a given redshift for several mass intervals (wider lines referring to more massive systems). Only results for masses above our 75% completeness level at each redshift are shown.

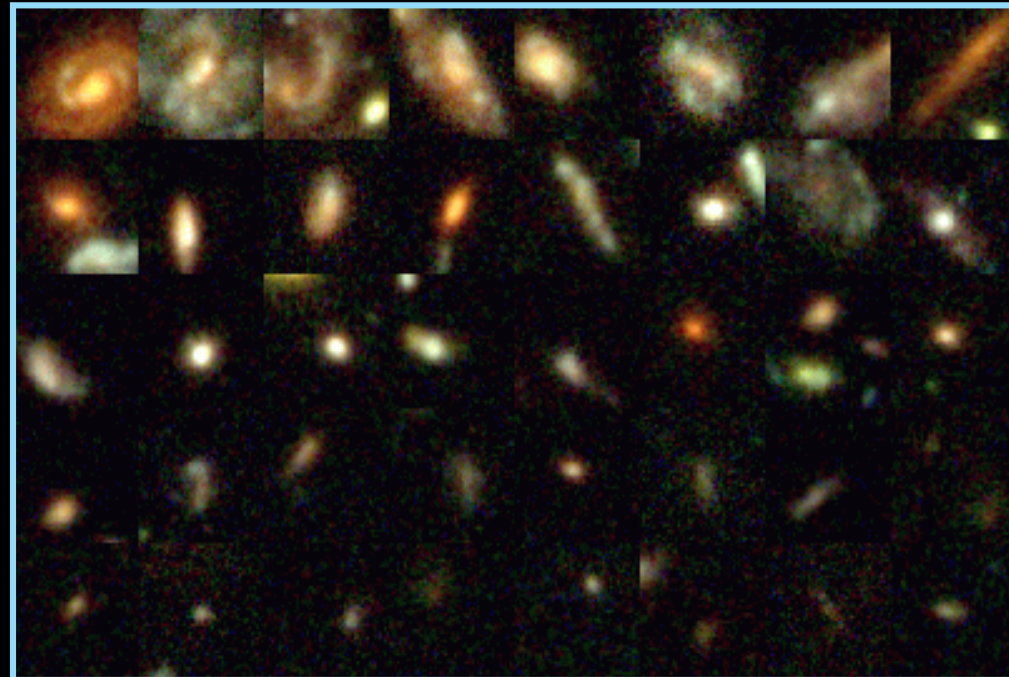
# 4. Massive galaxies finished SF earlier



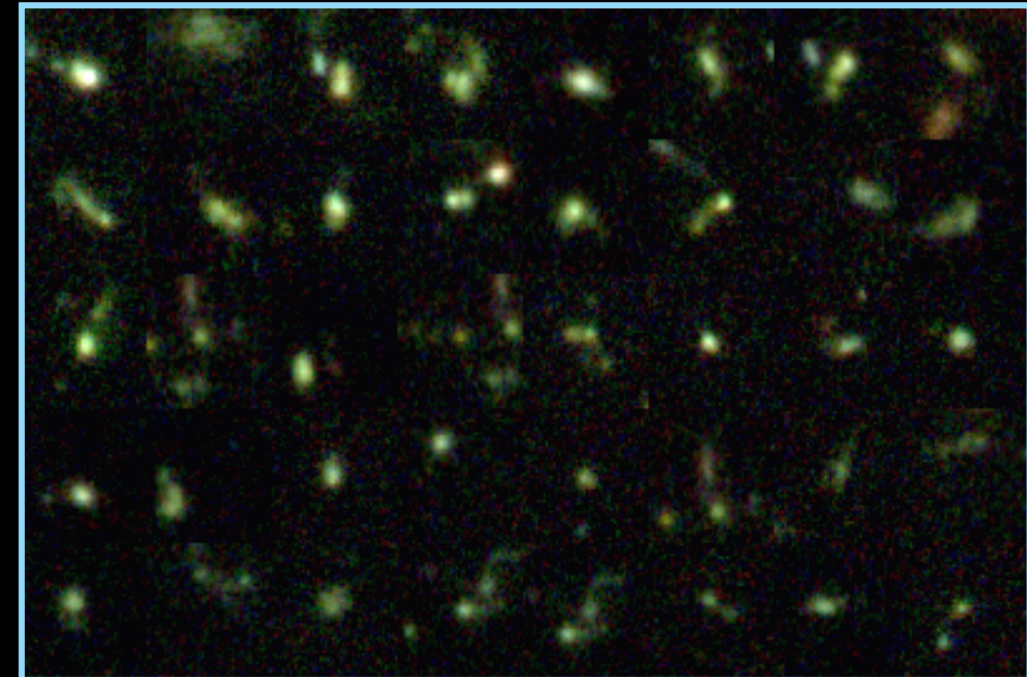
Can be seen in  
evolution of  
the stellar mass  
function

Madau & Dickinson ARAA 2014

## 5. Galaxy morphologies settle out sometime between $z=2$ and $z=1$



$z=1.07$



$z=2.50$

# Sorted by decreasing luminosity at fixed $z \rightarrow$

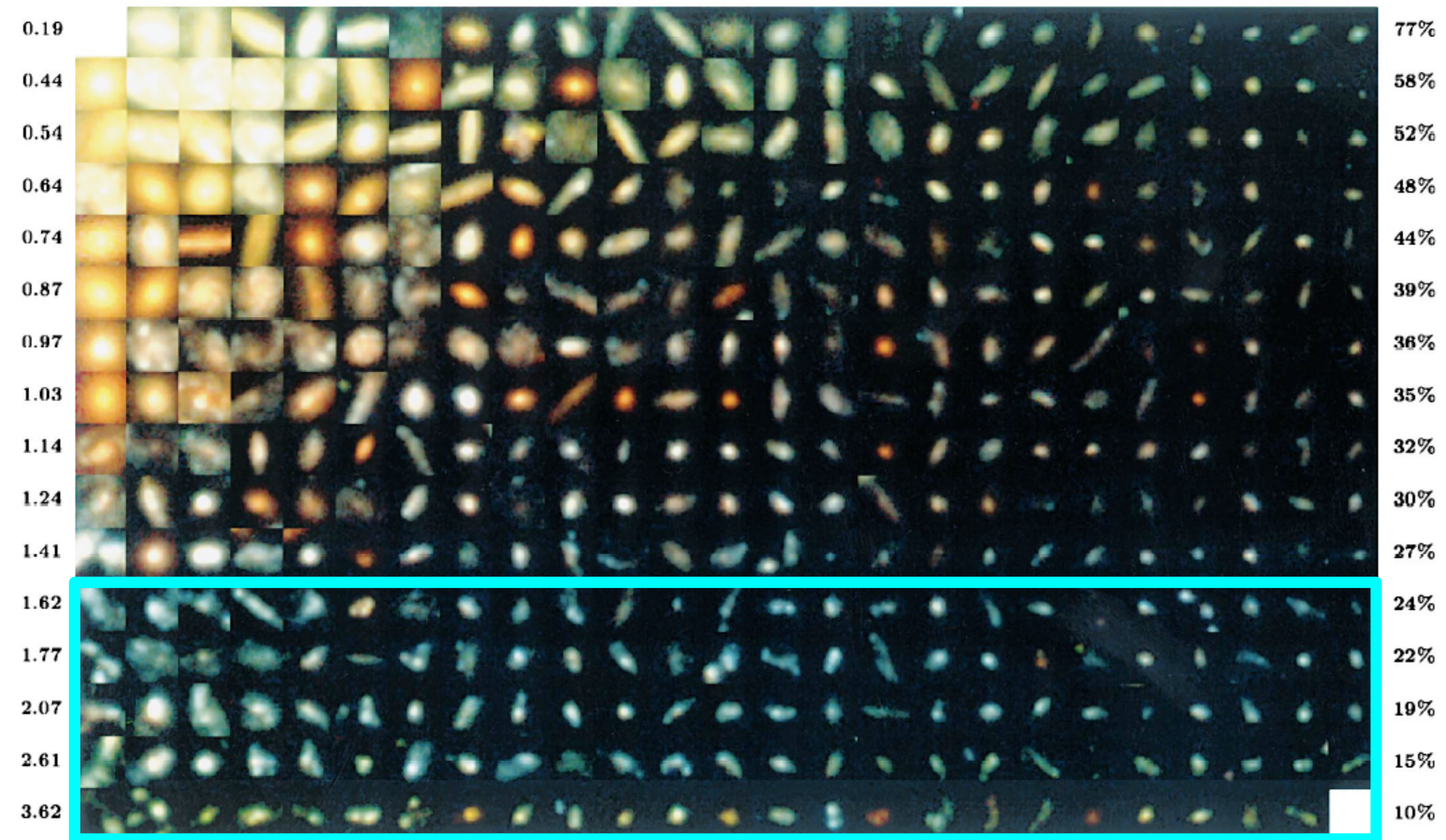
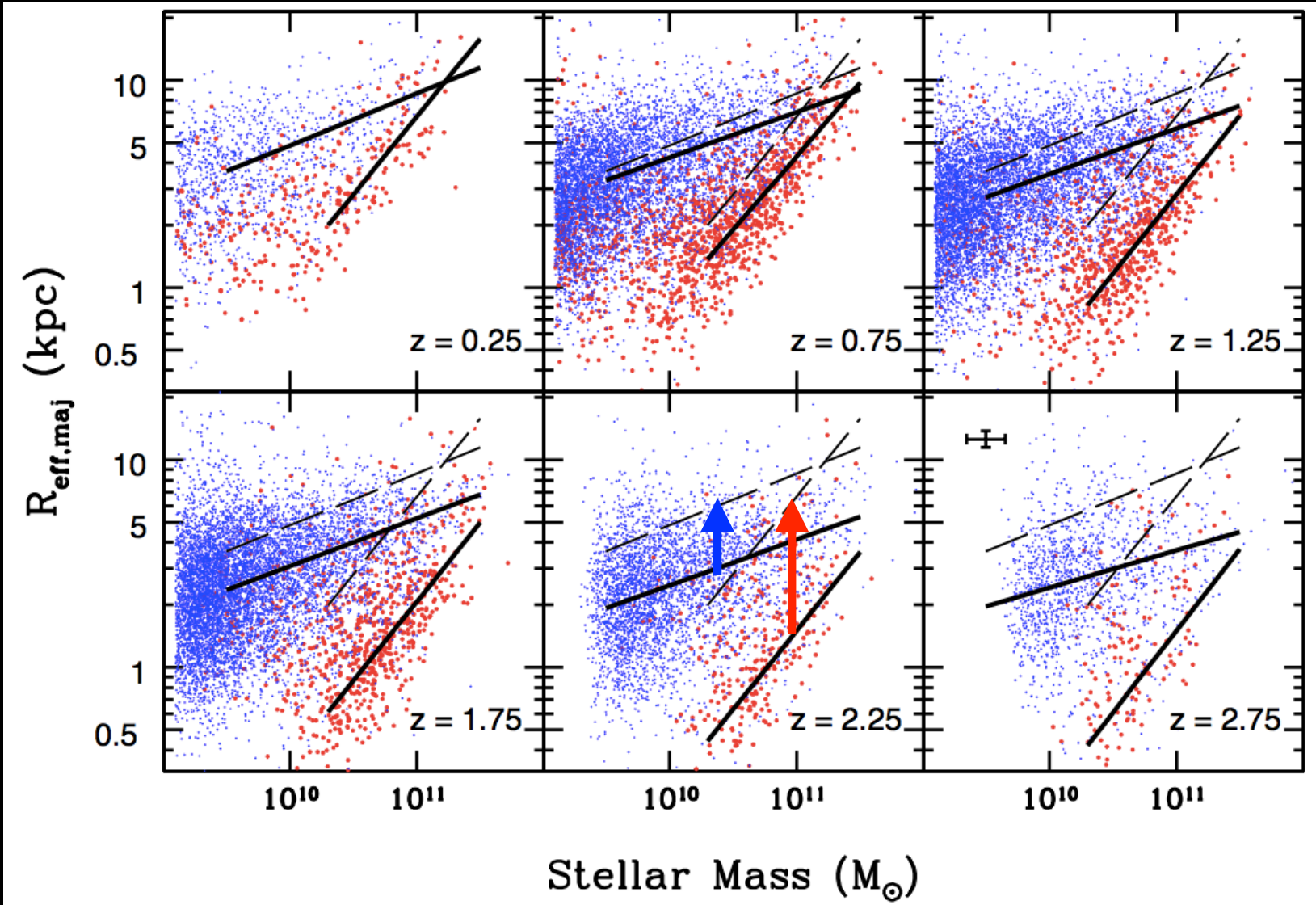


Photo-z's of HDF galaxies: Driver et al 1998

FIG. 3.—Hubble Deep Field photometric redshift sample. The sample is first sorted into redshift and divided into 16 redshift bins, each containing 25 galaxies. Within each redshift interval the galaxies are then ordered in terms of apparent magnitude (and therefore crudely in absolute magnitude). The progression down the page qualitatively reflects the process of galaxy evolution, although of course it does not correct for  $k$ -corrections and the redshift-dependent selection windows.

# 6. The sizes of galaxies grow with time

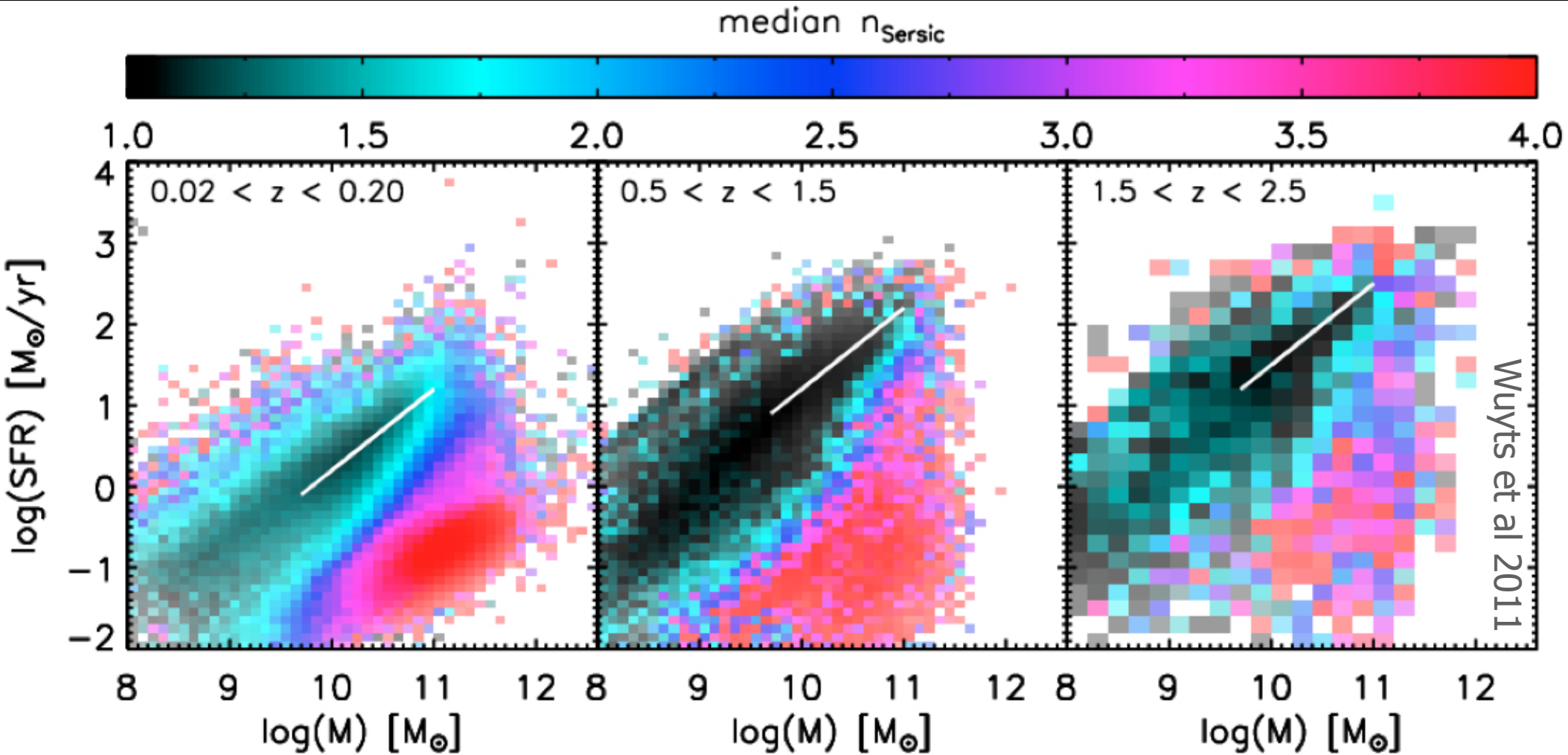


- Typical SF galaxy size increases slowly
- Typical red galaxy size increases rapidly

Figure 5. Size-stellar mass distribution of late- and early-type galaxies (same symbols as in Figure 2). A typical  $1\sigma$  error bar for individual objects in the higher-redshift bins is shown in the bottom-right panel. The lines indicate model fits to the early- and late-type galaxies as described in Section 3.1. The dashed lines, which are identical in each panel, represent the model fits to the galaxies at redshifts  $0 < z < 0.5$ . The solid lines represent fits to the higher-redshift samples. The mass ranges used in the fits are indicated by the extent of the lines in the horizontal direction. Strong evolution in the intercept of the size-mass relation is seen for early-type galaxies and moderate evolution is seen for the late-type galaxies (also see Figure 6). There is no significant evidence for evolution in the slope (also see Figure 6). The

van der Wal 2015

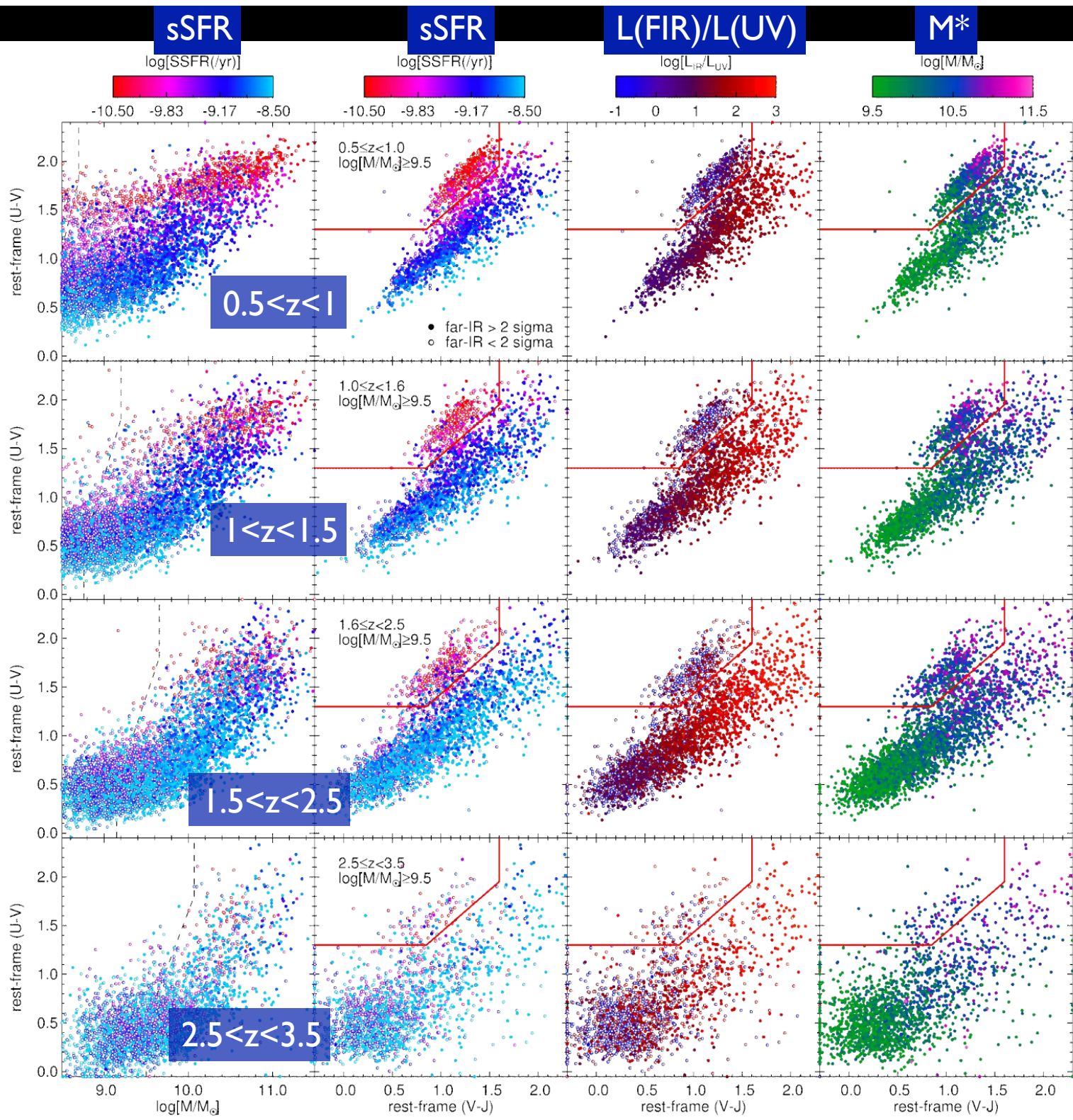
# 7. A star forming blue sequence exists out to $z \sim 1-2$



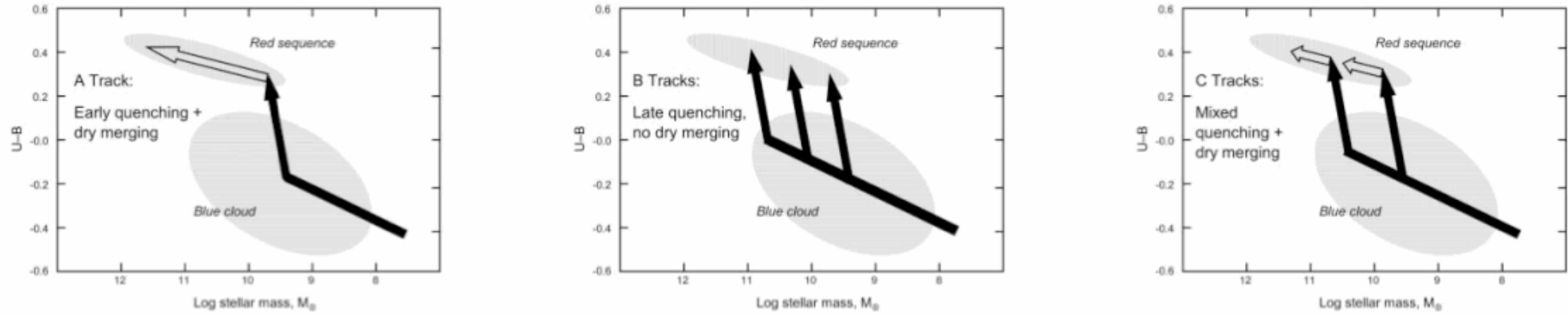
Surface brightness profile shape in the Star formation rate – Mass diagram. A structurally distinct "main sequence" of star-forming galaxies is clearly present at all observed epochs, and well approximated by a constant slope of 1 and a zeropoint that increases with lookback time (white line). While star-forming galaxies on the main sequence are well characterized by exponential disks, quiescent galaxies at all epochs are better described by cuspier, De Vaucouleurs profiles. Galaxies that occupy the tip and upper envelope of the main sequence also have cuspier light profiles, intermediate between main sequence galaxies and red and dead systems.

Narrowness of sequence suggests bursts of SF are not dominant form of mass growth (Noeske et al 2007)

Passive galaxies are not common earlier than  $z \sim 2.5$



# 8. Galaxies move onto the red sequence after $z \sim 1$ -2(?)

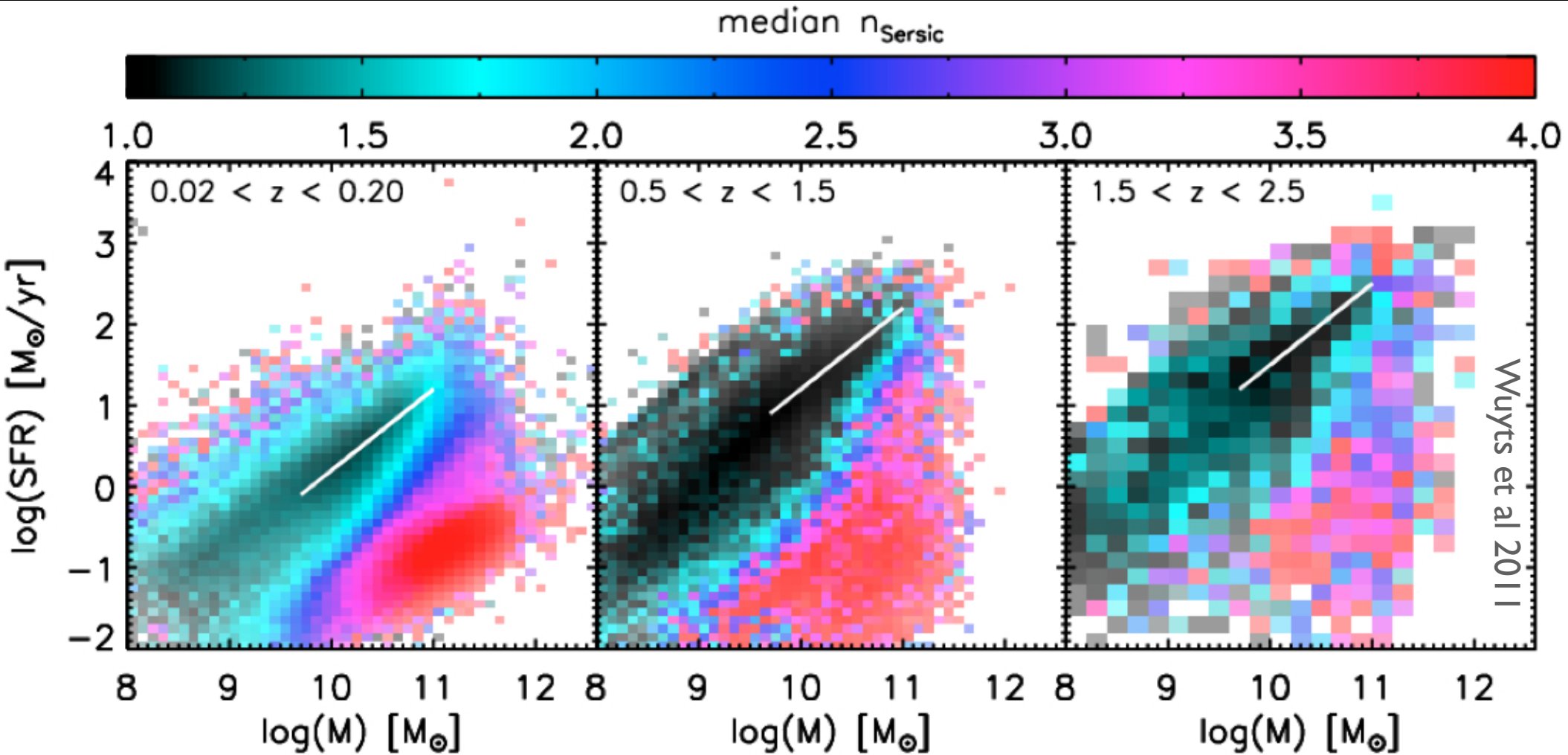


Faber et al 2007

FIG. 10.—Schematic arrows showing galaxies migrating to the red sequence under different versions of the merging hypothesis. Evolutionary tracks are plotted in the color-mass diagram. Here it is assumed that red galaxies arise from blue galaxies when star formation is quenched during a major merger, causing the galaxy to double its mass, but the exact nature of the quenching mechanism is not crucial. Quenching tracks are shown by the nearly vertical black arrows. The mergers would be gas-rich (“wet”) because the progenitor galaxies are blue objects making stars and hence contain gas. Once a galaxy arrives on the red sequence, it may evolve more slowly along it through a series of gas-poor, or “dry,” mergers. These are shown as the white arrows. They are tilted upward to reflect the aging of the stellar populations during the more gradual dry merging. A major variable is the time of mass assembly vs. the time of quenching. Three possibilities are shown. Track A represents very early quenching while the fragments of the galaxy are still small. In that case, most mass assembly occurs in dry mergers along the red sequence. Track B is the other extreme having maximally late quenching. In that case, galaxies assemble most of their mass while still blue and then merge once to become red with no further dry merging. Track C is intermediate, with contributions from both mechanisms. This “mixed” scenario best matches the properties of both distant and local ellipticals. In addition to the merging scenario illustrated here, the gas supply of some disks may simply be choked off or stripped out without mergers, to produce disk S0s. Such tracks would be vertical, but aside from this their histories are similar. S0s dominate on the red sequence below  $L^*$ , ellipticals above (Marinoni et al. 1999).

- Many possible routes to evolution onto red sequence
- Important to test for consistency with entire population

# 9. Out to $z \sim 1$ -2, the red sequence galaxies are morphologically $n=4$

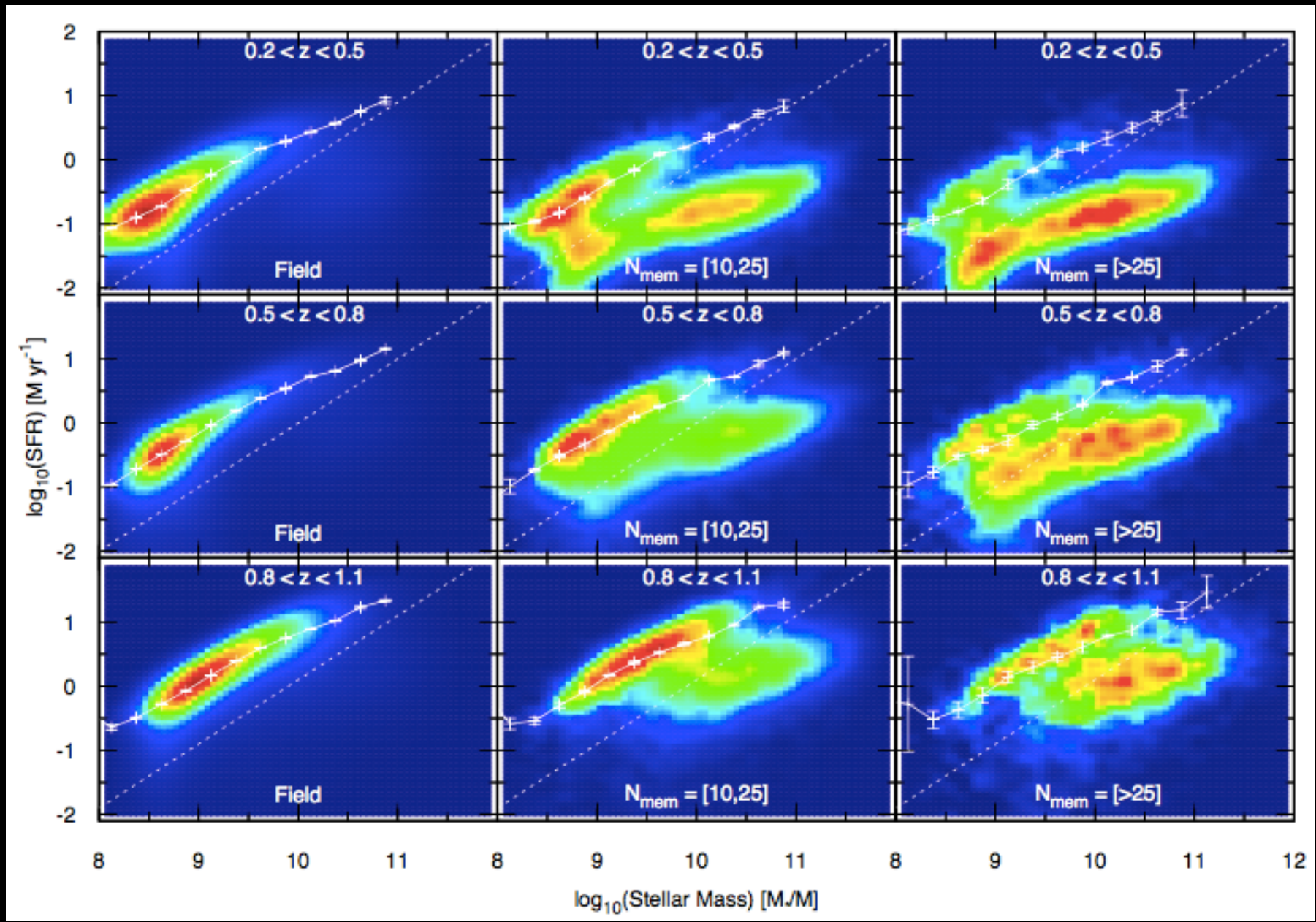


Surface brightness profile shape in the Star formation rate – Mass diagram. A structurally distinct "main sequence" of star-forming galaxies is clearly present at all observed epochs, and well approximated by a constant slope of 1 and a zeropoint that increases with lookback time (white line). While star-forming galaxies on the main sequence are well characterized by exponential disks, quiescent galaxies at all epochs are better described by cuspier, De Vaucouleurs profiles. Galaxies that occupy the tip and upper envelope of the main sequence also have cuspier light profiles, intermediate between main sequence galaxies and red and dead systems.

Narrowness of sequence suggests bursts of SF are not dominant form of mass growth (Noeske et al 2007)

# 10. Evolution varies w/ environment

Decreasing redshift ↑



Field Galaxies

Poor Clusters

Rich Clusters

Hyper Suprime Cam; Jian et al 2017

# Big issues

- Much of the evolution appears set by the galaxy halo mass.
- Why?
- What are the roles of AGN feedback (& black hole growth) and why are they coupled to galaxy halo mass?
- Why exactly does feedback shut down SF?
- Different evolution of “centrals” and “satellites”